© 2016. Published by The Company of Biologists Ltd | Development (2016) 143, 3154-3167 doi:10.1242/dev.139634

RESEARCH ARTICLE

Splice variants of the SWR1-type nucleosome remodeling factor Domino have distinct functions during *Drosophila melanogaster* oogenesis

Kenneth Börner and Peter B. Becker*

ABSTRACT

SWR1-type nucleosome remodeling factors replace histone H2A by variants to endow chromatin locally with specialized functionality. In *Drosophila melanogaster* a single H2A variant, H2A.V, combines functions of mammalian H2A.Z and H2A.X in transcription regulation and the DNA damage response. A major role in H2A.V incorporation for the only SWR1-like enzyme in flies, Domino, is assumed but not well documented *in vivo*. It is also unclear whether the two alternatively spliced isoforms, DOM-A and DOM-B, have redundant or specialized functions. Loss of both DOM isoforms compromises oogenesis, causing female sterility. We systematically explored roles of the two DOM isoforms during oogenesis using a cell type-specific knockdown approach. Despite their ubiquitous expression, DOM-A and DOM-B have non-redundant functions in germline and soma for egg formation. We show that chromatin incorporation of H2A.V in germline and somatic cells depends on DOM-B, whereas global incorporation in endoreplicating germline nurse cells appears to be independent of DOM. By contrast, DOM-A promotes the removal of H2A.V from stage 5 nurse cells. Remarkably, therefore, the two DOM isoforms have distinct functions in cell type-specific development and H2A.V exchange.

KEY WORDS: Chromatin, Remodeling, Histone variants, H2A.Z, H2A.X, HIS2AV, Germline

INTRODUCTION

The local replacement of nucleosomal histone H2A by variants is an evolutionarily conserved principle that endows chromatin with structural and functional diversity (Bönisch and Hake, 2012; Talbert and Henikoff, 2010). Two H2A variants can be considered as universal since they are found in all eukaryotes: H2A.Z and H2A.X. Currently, H2A.X is best known for the role of its phosphorylated form in DNA damage signaling. H2A.Z most likely has a role in regulating transcription, as it marks the nucleosomes next to promoters. Curiously, *Drosophila melanogaster* only has a single H2A variant, H2A.V, which combines the functions of H2A.Z and H2A.X as an architectural element downstream of active promoters, in heterochromatin organization and, in its phosphorylated form (γH2A.V), in the DNA damage response (Baldi and Becker, 2013).

H2A variants are incorporated by evolutionarily conserved SWR1-like remodeling enzymes, which use the energy freed by ATP hydrolysis to disrupt canonical nucleosomes. SWR1 enzymes share an N-terminal HSA domain and a spacer region that splits the conserved ATPase domain, enabling unique regulation mechanisms (Morrison and Shen, 2009). Mammals utilize two SWR1-like enzymes: p400 (or Ep400) and SRCAP (Cai et al., 2005; Eissenberg et al., 2005; Jin et al., 2005; Ruhl et al., 2006). By contrast, the *D. melanogaster* genome only contains a single SWR1-like enzyme gene: *domino* (*dom*) (Ruhf et al., 2001). Alternative splicing of the *dom* transcript produces two major isoforms, DOM-A and DOM-B (Ruhf et al., 2001), which differ in their C-termini. The DOM-A isoform features poly-glutamine (poly-Q) stretches and a SANT domain, whereas the DOM-B C-terminus is largely unstructured (Eissenberg et al., 2005; Ruhf et al., 2001). Early reports found DOM-B to be rather ubiquitously expressed, but DOM-A was detected only in the embryonic nervous system, larval salivary glands and S2 cells (Eissenberg et al., 2005; Messina et al., 2014; Ruhf et al., 2001), suggesting distinct functions for the two isoforms.

SWR1-like remodelers typically reside in multi-subunit complexes (Morrison and Shen, 2009), but little is known about DOM-containing complexes. DOM-A has been purified from S2 cells as part of a 16-subunit assembly that also contains the acetyltransferase TIP60, apparently combining features of the yeast SWR1 remodeling and NuA4 acetyltransferase complexes (Kusch et al., 2004). Likewise, our understanding of the roles of DOM enzymes in H2A.V exchange *in vivo* is anecdotal. DOM has been linked to H2A.V incorporation at the *E2f* promotor (Lu et al., 2007). It has also been suggested that H2A.V exchange requires prior acetylation by TIP60 (Kusch et al., 2004, 2014).

Previous genetic analyses characterized *dom* as required for cell proliferation and viability, homeotic gene regulation and Notch signaling (Eissenberg et al., 2005; Ellis et al., 2015; Gause et al., 2006; Kwon et al., 2013; Lu et al., 2007; Ruhf et al., 2001; Sadasivam and Huang, 2016; Walker et al., 2011), but did not attempt to resolve distinct functions of the two isoforms. *dom* is essential for fly development (Ruhf et al., 2001) and *dom* mutants die during pupariation (Braun et al., 1998; Ruhf et al., 2001). Furthermore, oogenesis in adult flies is strongly perturbed, causing sterility (Ruhf et al., 2001).

D. melanogaster oogenesis provides an excellent opportunity to study self-renewal and differentiation of germline and somatic stem cells (GSCs and SSCs, respectively) in the context of egg chamber morphogenesis (Hudson and Cooley, 2014; Ting, 2013; Yan et al., 2014). The formation of eggs starts in the germarium at the anteriormost end of an ovariole. There, two to three GSCs divide asymmetrically to self-renew and shed a daughter cystoblast. This cell initiates four mitotic divisions with incomplete cytokinesis to form an interconnected 16-cell cyst. One particular cell of a cyst is determined to become the oocyte and the remaining 15 cells

Biomedical Center and Center for Integrated Protein Science Munich, Ludwig-Maximilians-University, Großhaderner Strasse 9, 82152 Munich, Germany.

*Author for correspondence (pbecker@med.uni-muenchen.de)

P.B.B., 0000-0001-7186-0372

Received 11 May 2016; Accepted 21 July 2016

Development (2016) 143, 3154-3167 doi:10.1242/dev.139634

transform into polyploid nurse cells by endoreplication. In parallel, SSCs produce somatic follicle cells, which encapsulate cysts to form individual egg chambers. Oogenesis further runs through 14 stages of egg chamber development to produce a functional egg.

It is not surprising that nucleosome remodeling factors have been found to be important for oogenesis given the widespread requirement for chromatin plasticity during development (Chioda and Becker, 2010; Ho and Crabtree, 2010; Iovino, 2014). Interestingly, an RNA interference (RNAi) screen identified DOM as important for GSC self-renewal and cystoblast differentiation (Yan et al., 2014). DOM function is also essential for SSC self-renewal (Xi and Xie, 2005). The mechanisms of DOM function in these processes are unclear, but involvement of H2A.V exchange has been suggested. H2A.V signals show a modest decrease in *dom* mutant GSC clones in *D. melanogaster* testes (Morillo Prado et al., 2013) and are not detectable in mutant germline clones for MRG15, a DOM-A/TIP60 complex subunit (Joyce et al., 2011). Yet, direct evidence for a role of DOM – and specific roles for each isoform – in H2A.V incorporation during oogenesis is lacking.

We used a cell type-specific RNAi approach to dissect the functions of DOM-A and DOM-B during *D. melanogaster* oogenesis. Our analysis suggests non-redundant requirements for both DOM isoforms in several cell differentiation programs and for H2A.V exchange.

RESULTS

Expression of both DOM splice variants in *D. melanogaster* ovarioles

DOM is ubiquitously expressed in the female germline of *D. melanogaster* ovarioles (Yan et al., 2014), but other studies suggest expression of only DOM-B in soma and germline cells (Ruhf et al., 2001; Xi and Xie, 2005). Owing to the lack of specific DOM-A and DOM-B antibodies for immunofluorescence microscopy we generated transgenes expressing GFP-3×FLAG-tagged DOM from a recombined fosmid using the flyfosmid recombineering technique (Ejsmont et al., 2009). This way, we obtained fly lines expressing N-terminally tagged DOM (*GFP-dom*) and C-terminally tagged DOM-A (*dom-A-GFP*) and DOM-B (*dom-B-GFP*) from its chromosomal regulatory context (Fig. 1A,B). The latter two constructs express one tagged isoform, while the other is untagged. As a control, we replaced the *dom* locus with the GFP-3×FLAG cassette (Δ*dom-GFP*) (Fig. 1B).

We complemented lethality and sterility of two *dom* alleles to assess the functionality of the *dom* transgenes. Viable homozygous dom^1 or dom^9 fly lines were obtained by complementation with the *dom* transgenes (Fig. S1A). By contrast, the Δ*dom-GFP* transgene did not rescue pupal lethality in the dom^1 allele and compromised viability in the dom^9 allele (Fig. S1A). Furthermore, a characteristic larval phenotype of dom^1 mutants (Braun et al., 1998; Ruhf et al., 2001) was completely rescued by the *dom* transgenes (Fig. S1B,C). Importantly, egg laying capacity was restored to wild-type levels in homozygous dom^9 females complemented with the *dom* transgenes, but not by the Δ*dom-GFP* transgene (Fig. 1C). Our analysis provides the first comprehensive validation of *dom* allele phenotypes using complementation with *dom* transgenes.

Western blotting using the FLAG antibody showed expression of *dom* transgenes in ovaries (Fig. 1D) and larval brains (Fig. S1D) (Ruhf et al., 2001). We confirmed the ubiquitous expression of DOM-B in germline and somatic cells of ovarioles with the GFP antibody (Fig. 1F) (Ruhf et al., 2001; Xi and Xie, 2005). The specificity of antibody was confirmed as wild-type ovarioles showed only background staining (Fig. 1H). Interestingly, we also observed expression of DOM-A in germline and somatic cells of ovarioles (Fig. 1E). Both DOM isoforms were present in GSCs, cystoblasts, SSCs and follicle cells, with enrichment in oocyte nuclei in comparison to nurse cells (Fig. 1E,F). Nuclear localization was not due to the GFP tag since GFP expressed from the Δ*dom-GFP* transgene showed only cytoplasmic signal (Fig. 1G). In summary, DOM-A and DOM-B are expressed in germline and somatic cells during oogenesis.

Cell type-specific knockdown of DOM-A and DOM-B reveals requirements during fly development

To dissect the cell type-specific requirements for DOM-A and DOM-B we induced RNAi by expressing small hairpin (sh) RNA directed against *dom* under the control of the Gal4/UAS system (Ni et al., 2011). We also generated transgenic flies expressing shRNA directed selectively against each individual DOM isoform and compared the resulting phenotypes with corresponding depletions of H2A.V and TIP60. *GFP* shRNA served as a control for non-specific effects.

The effect of ubiquitous depletion of DOM should resemble the lethal phenotype of the dom^1 allele (Ruhf et al., 2001). Indeed, we observed pupal lethality upon expression of *dom-1* shRNA with an *actin-Gal4* driver, whereas siblings lacking the driver were not affected (Fig. 2A). Remarkably, individual depletion of DOM-A or DOM-B led to pupal lethality, indicating essential functions for each isoform during fly development (Fig. 2A).

DOM and other TIP60 complex subunits are well known as positive regulators of Notch signaling in wing formation (Eissenberg et al., 2005; Ellis et al., 2015; Gause et al., 2006; Kwon et al., 2013). We also scored typical Notch phenotypes, such as defective wing margins and wing nicks, with high penetrance upon expression of two *dom* shRNAs from the *C96-Gal4* driver (Fig. S2). Interestingly, the two DOM isoforms appear to have distinct functions in wing development since *dom-A* shRNA led to wing margin phenotypes with high penetrance, whereas *dom-B* shRNA had only minor effects (Fig. S2).

To document the efficiency and specificity of RNAi depletion we raised monoclonal antibodies against peptides of DOM-A (DOA1) and DOM-B (DOB2) for western blot detection. No DOM signals were detected in larval brain extracts with DOA1 and DOB2 antibodies upon *dom-1* shRNA depletion driven by *elav-Gal4* (Fig. 2B). Furthermore, signals for multiple DOM-A bands and DOM-B were strongly reduced upon depletion with *dom-A* and *dom-B* shRNAs, respectively (Fig. 2B). Multiple DOM-A bands have been reported previously (Kusch et al., 2004; Ruhf et al., 2001) and might reflect additional minor DOM-A isoforms or low-level degradation. As a control, levels of the SWI2/SNF2 ATPase ISWI were unaltered (Fig. 2B).

Despite all efforts, the monoclonal DOM-A and DOM-B antibodies could not be used for immunofluorescence microscopy applications. Alternatively, we combined GFP-tagged *dom* transgenes with shRNA constructs expressed from the *traffic jam-Gal4* driver, which is specifically expressed in somatic follicle cells but not in germline nurse cells (Olivieri et al., 2010). As a control, we detected the *dom* transgenes in follicle and nurse cells using the GFP antibody (Fig. 2C,I). We did not detect GFP signal in follicle cell nuclei upon *dom-1*, *dom-A* and *dom-B* shRNA depletion in the respective *GFP-dom*, *dom-A-GFP* and *dom-B-GFP* transgenes (Fig. 2D,E,G,I). However, GFP signal was detected in nurse cell nuclei of the same egg chambers (Fig. 2D,E,G). Importantly, DOM-A or DOM-B depletion did not affect the localization and levels of the other isoform (Fig. 2F,H,I and Fig. S3), arguing for an

Development (2016) 143, 3154-3167 doi:10.1242/dev.139634

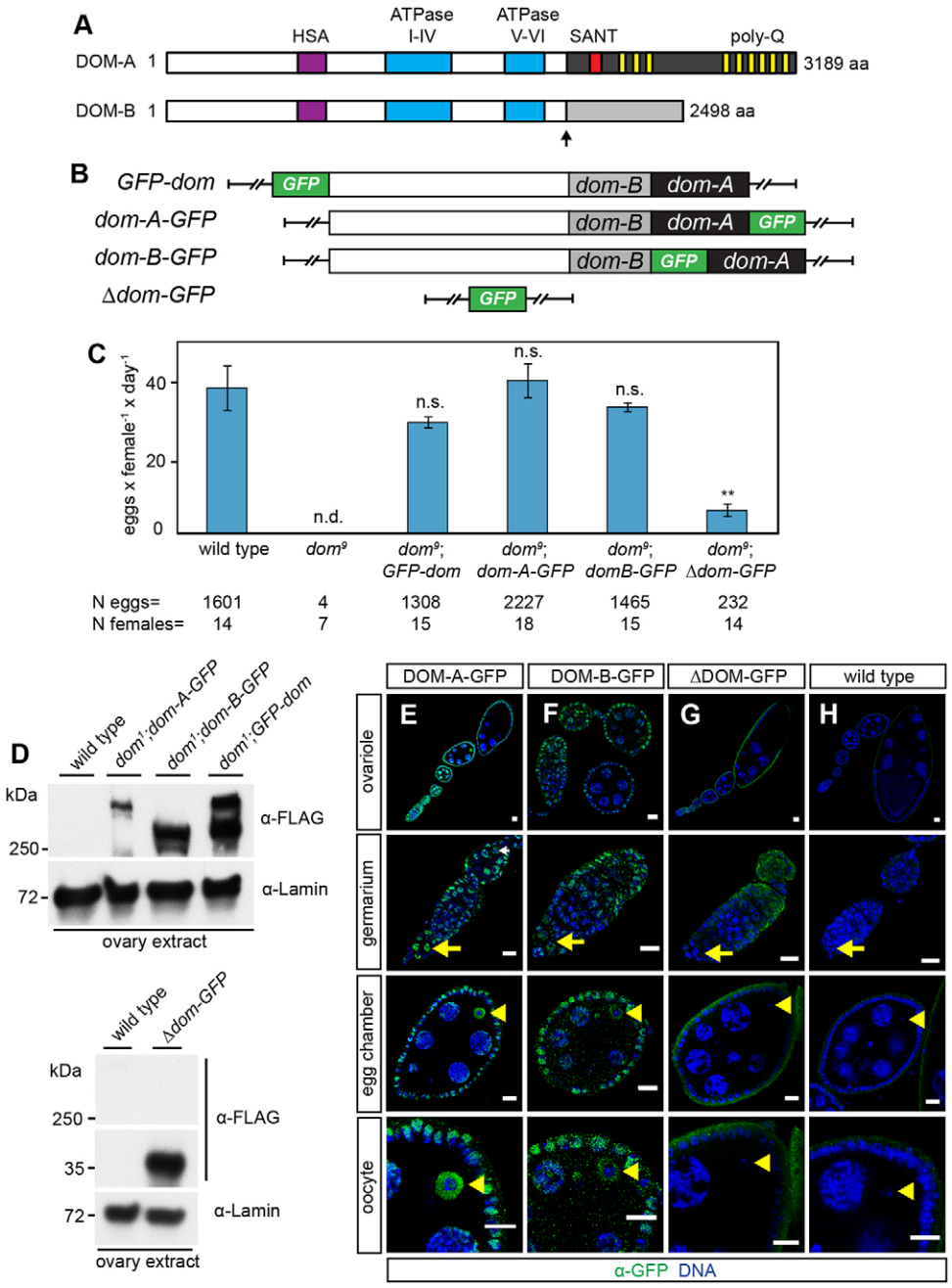

Fig. 1. Ubiquitous expression of DOM-A and DOM-B in *D. melanogaster* ovarioles. (A) Schematic representation of DOM isoforms. Arrow indicates the different C-terminal regions in DOM-A (dark gray) and DOM-B (light gray). Purple, blue, red and yellow rectangles represent HSA, ATPase, SANT and poly-Q domains, respectively. (B) Schematic representation of the *dom* fosmid constructs. White, dark gray and light gray rectangles represent the 5′ genomic region of *dom* and splice variant of *dom-A* or *dom-B*, respectively. Green rectangle indicates the inserted 2×TY1-sGFP-3×FLAG tag. (C) Complementation of the dom^{9} allele with *dom* transgenes rescues the sterility phenotype. Quantification of egg laying capacity is shown. The data show mean values of eggs laid per female per day with s.d. of three biological replicates. *N* eggs represents the total number of scored eggs and *N* females the total number of analyzed females. $^{**}P<0.01$; n.s., not significant. Two-tailed Student's *t*-test compared with wild type. n.d., not determined. (D) Western blot from ovaries probed with anti-FLAG is shown for the following homozygous genotypes: wild type, dom^{1};*dom-A*, dom^{1};*dom-B*, dom^{1};*GFP-dom*. Lamin signal served as a loading control. (E-H) Immunofluorescence images of different oogenesis stages with staining of GFP (green) and DNA (blue) for the following homozygous genotypes: (E) *dom-A-GFP*, (F) *dom-B-GFP*, (G) Δ*dom-GFP* fosmid and (H) wild type. Arrows and arrowheads indicate germline stem cells (GSCs) and oocyte nuclei, respectively. Scale bars: 10 µm.

independent localization of the two DOM isoforms. Furthermore, TIP60 depletion did not affect DOM-A or DOM-B localization (Fig. S4). We conclude that shRNAs against *dom*, *dom-A* and *dom-B* specifically and efficiently deplete their corresponding target protein.

Loss of DOM-A in germline cells leads to early cystoblast defects, while loss of DOM-B generates defective late egg chambers

Previous analysis could not reveal the specific contributions of DOM-A and DOM-B function to germline development (Ruhf et al., 2001; Yan et al., 2014). We confirmed the importance of DOM for fertility by scoring the egg laying capacity of F1 females from crosses of different *dom* shRNAs with the germline-specific *MTD-Gal4* driver (Fig. 3A) (Yan et al., 2014). We found the egg laying capacity strongly impaired upon separate depletion of DOM isoforms, an effect that was similar if the H2A.V variant was depleted (Fig. 3B,C). *Tip60* shRNAs showed moderately decreased egg laying capacity (Fig. 3C).

We stained ovaries of knockdown animals for the germline-specific cytoplasm marker Vasa and the follicle cell-specific adhesion molecule Fasciclin III (Fig. 3D-I). As expected, depletion with *dom-1* shRNA led to an agametic phenotype with characteristic small ovaries and defects in cyst differentiation in the germarium (Fig. 3E) (Yan et al., 2014). The effects of depleting DOM-A and H2A.V resembled this phenotype (Fig. 3F,H). By contrast, germline development in the germarium appeared normal upon DOM-B and TIP60 depletion (Fig. 3G,I), but many defective late egg chambers were observed (Fig. 3G,I). We conclude that the two DOM isoforms are both required for proper oogenesis, but that

Development (2016) 143, 3154-3167 doi:10.1242/dev.139634

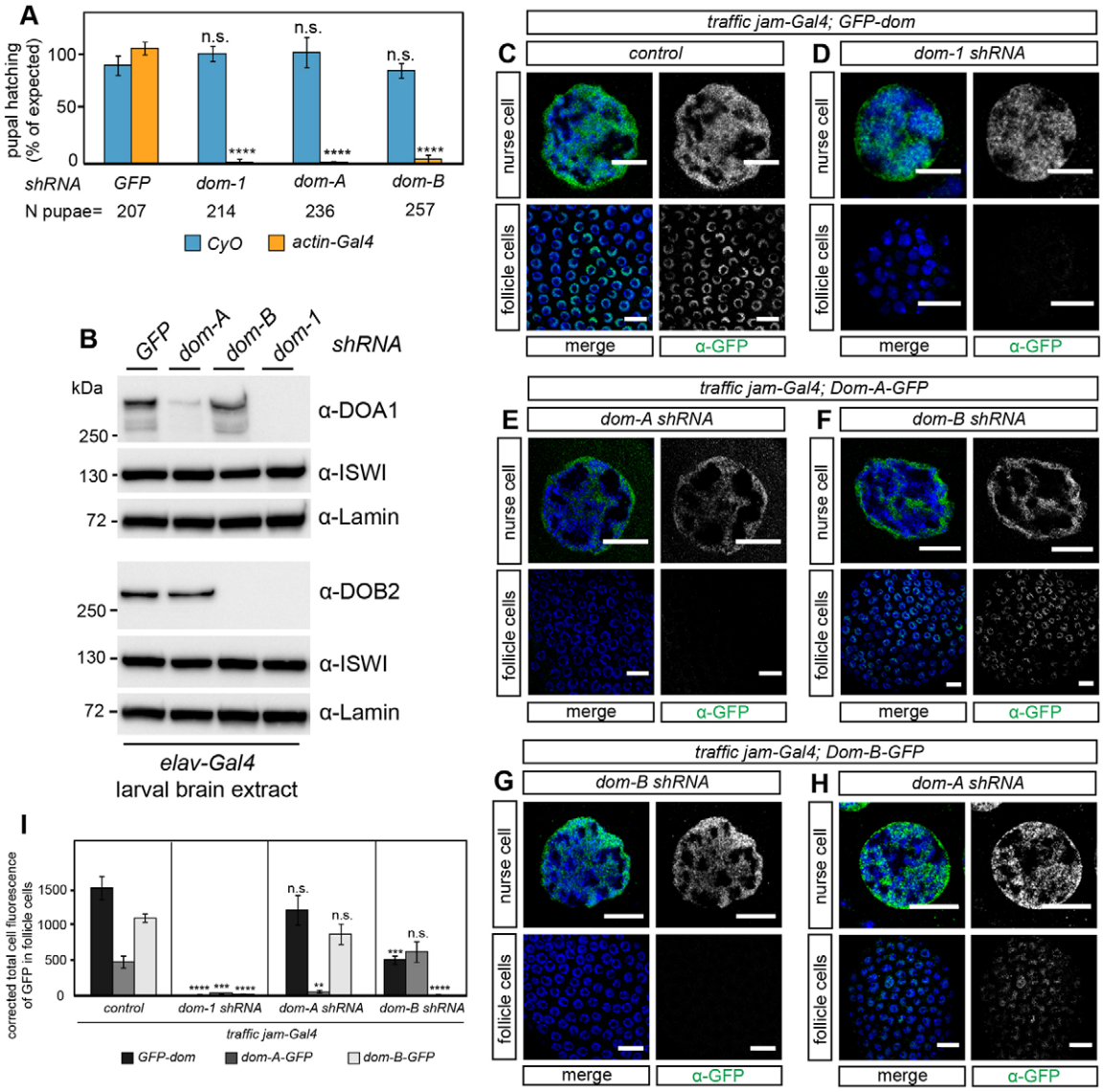

Fig. 2. Cell type-specific knockdown of DOM-A and DOM-B reveals requirements during fly development. (A) DOM-A and DOM-B are essential during fly development. *UAS-shRNA* males for *GFP*, *dom-1*, *dom-A* and *dom-B* were crossed with *actin-Gal4*/*CyO* driver females. Pupal hatching was determined as the observed to expected frequency of *CyO* and *actin-Gal4* F1 offspring. The data show mean values of percentage with s.d. from three biological replicates. *N* pupae represents the total number of pupae scored. Two-tailed Student's *t*-test for comparison of *CyO* or *actin-Gal4* siblings with *GFP* shRNA. (B) Validation of specificity for *dom-A* and *dom-B* shRNA knockdowns. *UAS-shRNA* males for *GFP*, *dom-1*, *dom-A* and *dom-B* were crossed with *elav-Gal4* females. F1 offspring larval brains are probed with DOA1 and DOB2 antibodies in western blot. Lamin and ISWI signals provided controls. (C-H) Validation of specificity of *dom-A* and *dom-B* shRNA knockdowns using transgenic *dom* fosmids. GFP-tagged *dom* transgenes are combined with *dom-1*, *dom-A* and *dom-B* shRNA constructs and the somatic follicle cell-specific driver *traffic jam-Gal4*. Representative immunofluorescence images of nurse and follicle cells with staining of GFP (green) and DNA (blue) are shown. Scale bars: 10 µm. See also Fig. S2. (I) Quantification of GFP signals in follicle cells of egg chambers. Corrected total cell fluorescence of GFP was calculated for ten follicle cells. Mean values with s.d. of three biological replicates are shown. Two-tailed Student's *t*-test for comparison of *dom-1*, *dom-A* or *dom-B* shRNA with control. ***P*<0.01, ****P*<0.001, *****P*<0.0001; n.s., not significant.

they differ in their requirements: DOM-A is essential for early germline development, whereas DOM-B is crucial for egg chamber development at later stages of oogenesis.

Loss of DOM-A or DOM-B in germline cells outside of the germarium leads to a 'dumpless' egg phenotype

DOM-B was required in germline cells for proper egg chamber development. The abundant defects in the germarium upon DOM-A depletion precluded the assessment of a similar role during later stages of oogenesis. Therefore, we combined the *matα4-Gal4* driver, which is specifically expressed in the germline from stage 1 egg chambers onwards (Fig. 4A) (Yan et al., 2014), with different *dom*, *H2A.V* and *Tip60* shRNAs and stained for Vasa and the cytoplasmic oocyte marker ORB. Notably, *matα4-Gal4*-directed knockdown did not affect the development of germarium and ovariole, but resulted in defective late egg chambers with short eggs and non-fragmented nurse cells characteristic of the 'dumpless' egg phenotype (Fig. 4B-G). Interestingly, individual loss of either DOM isoform or TIP60 led to 'dumpless' eggs comparable to DOM or H2A.V depletion (Fig. 4H,I) and accordingly to significantly reduced egg laying (Fig. 4J,K). We conclude that both DOM isoforms are required in germline cells outside of the germarium for egg chamber formation.

Development (2016) 143, 3154-3167 doi:10.1242/dev.139634

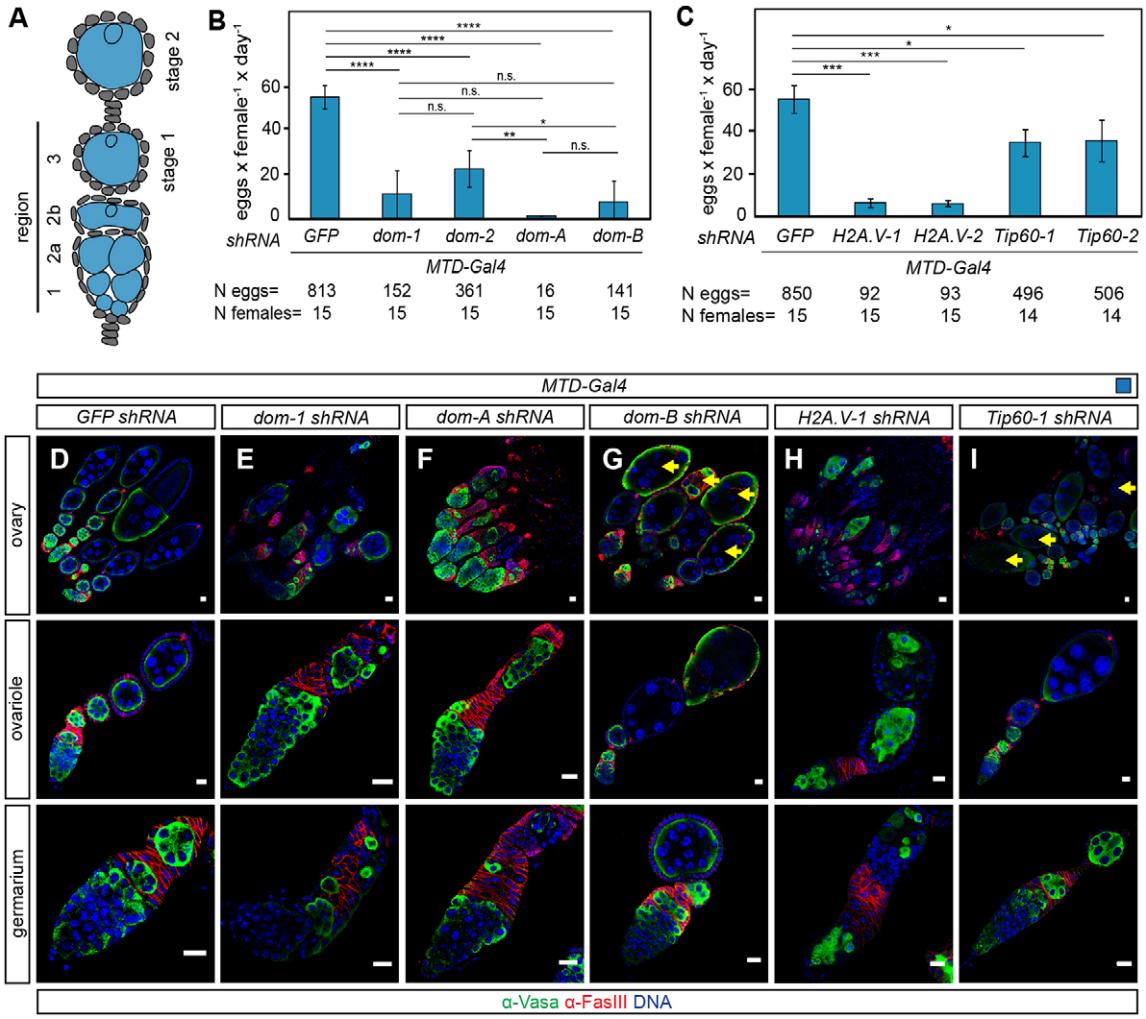

Fig. 3. Loss of DOM-A in germline cells leads to early cystoblast defects, while loss of DOM-B generates defective late egg chambers. (A) Diagram of the early stages of *D. melanogaster* oogenesis. The specific expression pattern of the *MTD-Gal4* driver in germline cells is highlighted in blue. (B,C) Quantification of egg laying capacity. The data show mean values of eggs laid per female per day with s.d. of three biological replicates. *N* eggs represents the total number of scored eggs and *N* females the total number of analyzed females. **P*<0.05, ***P*<0.01, ****P*<0.001, *****P*<0.0001; n.s., not significant. Two-tailed Student's *t*-test. (D-I) Immunofluorescence images of ovary, ovariole and germarium with staining of Vasa (green), Fasciclin III (red) and DNA (blue) for the following genotypes: *MTD-Gal4* with (D) *GFP*, (E) *dom-1*, (F) *dom-A*, (G) *dom-B*, (H) *H2A.V-1* and (I) *Tip60-1* shRNA. Arrows indicate defective late egg chambers. Scale bars: 10 µm.

Loss of DOM-A or DOM-B in somatic follicle cells leads to severe packaging defects

DOM function is not only required in the germline but is also essential for somatic follicle cell development (Xi and Xie, 2005). To address whether both DOM isoforms are also required for follicle cell function, we used the *traffic jam-Gal4* driver (Fig. 5G) in combination with different shRNAs. We scored severe packaging phenotypes upon DOM, DOM-A, DOM-B, TIP60 or H2A.V depletion, ranging from two cysts in a single egg chamber to complete ovariole fusions (Fig. 5A-F). Furthermore, many germaria showed additional stalk-like structures without germline cysts (Fig. 5H-K), indicating defects in the coordination of follicle cell proliferation with cyst differentiation. Remarkably, we observed egg chambers with abnormal cyst numbers ranging from one to more than 16 cells (Fig. 5A-F), suggesting a soma-dependent proliferation defect in the germline. Defective late egg chambers showed signals for activated Caspase 3 (Fig. 5L-O). As a result, egg laying capacity was drastically impaired (Fig. 5P). We validated packaging phenotypes and sterility with another somatic driver line, *c587-Gal4*, which is expressed in somatic escort cells and early follicle cells in the germarium (Fig. S5) (Eliazer et al., 2011; Kai and Spradling, 2003). We conclude that DOM-A and DOM-B function is crucial in somatic follicle cells for the proper packaging of egg chambers.

DOM-B promotes global H2A.V incorporation into germline chromatin of the germarium

In order to explore the roles of DOM isoforms in H2A.V incorporation into chromatin and in γH2A.V turnover *in vivo*, we raised a specific polyclonal antibody against an H2A.V peptide. We found H2A.V to be ubiquitously expressed in somatic and germline cells of the germarium with a notable enrichment in GSCs (Fig. 6A,B). Remarkably, H2A.V and γH2A.V signals were only detected in nurse cells up to stage 5 of oogenesis (Fig. 6C), and both signals were absent in later nurse cell nuclei (Fig. 6D). However, H2A.V was present in the surrounding follicle cells at all stages, providing convenient staining controls (Fig. 6A-D). These observations are in general agreement with previous studies (Joyce

Development (2016) 143, 3154-3167 doi:10.1242/dev.139634

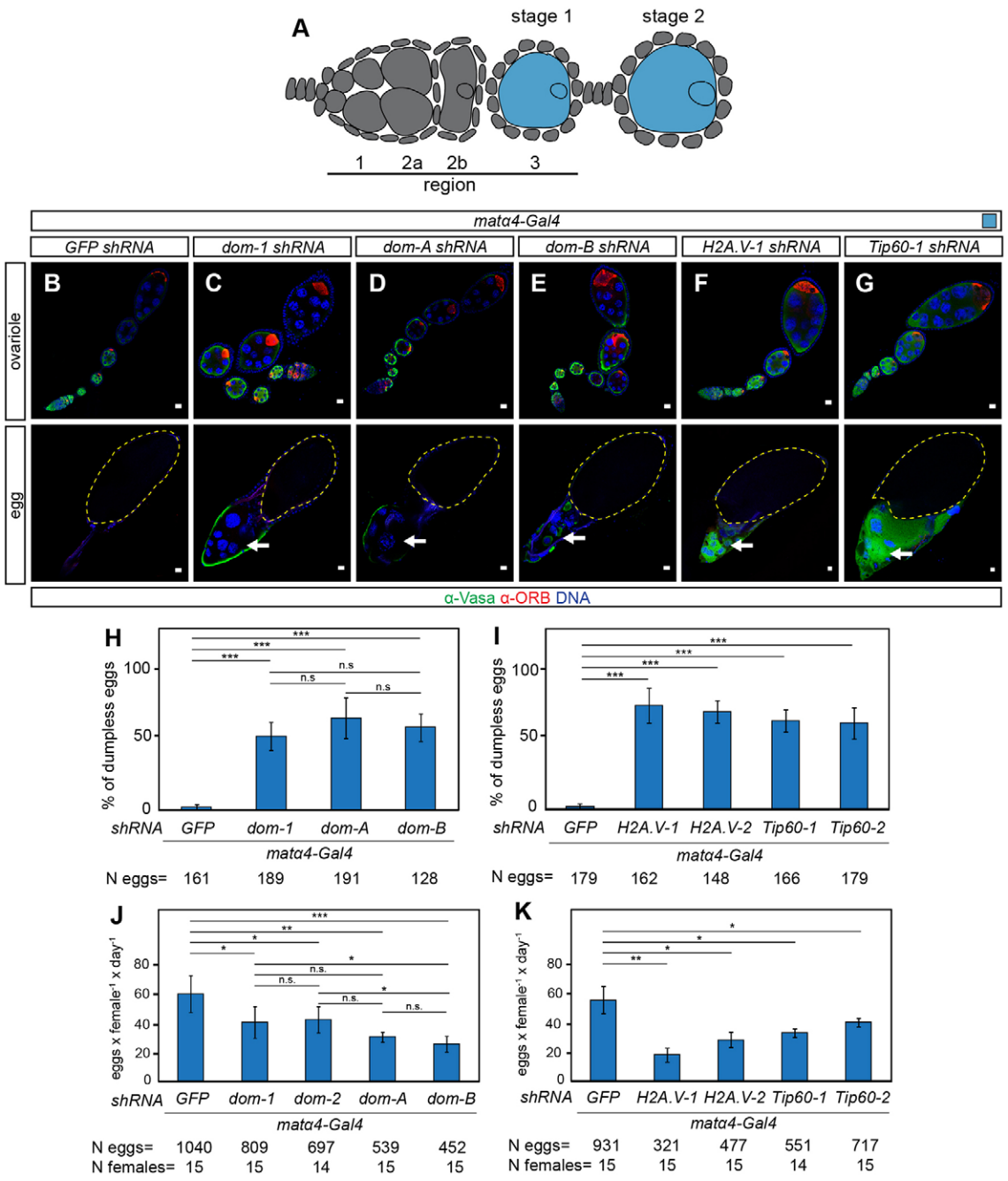

Fig. 4. Loss of DOM in germline cells outside the germarium leads to a 'dumpless' egg phenotype. (A) Diagram of the early stages of *D. melanogaster* oogenesis. The specific expression pattern of the *matα4-Gal4* driver in germline cells from stage 1 of oogenesis is highlighted in blue. (B-G) Immunofluorescence images of ovariole and egg with staining of Vasa (green), ORB (red) and DNA (blue) for the following genotypes: *matα4-Gal4* with (B) *GFP*, (C) *dom-1*, (D) *dom-A*, (E) *dom-B*, (F) *H2A.V-1* and (G) *Tip60-1* shRNA. Arrow indicates the anterior end of the egg chamber with non-fragmented nurse cells. Yellow dashed line indicates posterior egg. Scale bars: 10 µm. (H,I) Quantification of the 'dumpless' egg phenotype. The data show mean values in percentage with s.d. of three biological replicates. *N* eggs represents the total number of scored eggs. (J,K) Quantification of egg laying capacity. The data show mean values of eggs laid per female per day with s.d. of three biological replicates. *N* eggs represents the total number of scored eggs and *N* females the total number of analyzed females. **P*<0.05, ***P*<0.01, ****P*<0.001; n.s., not significant. Two-tailed Student's *t*-test.

et al., 2011), except that we did not detect signals for H2A.V in oocytes, possibly owing to differences in H2A.V epitope sequence.

Upon depletion of DOM and DOM-B with *MTD-Gal4* we found that H2A.V was lost specifically in germline cells of the germarium (Fig. 6F,H,L,M). H2A.V was essentially absent since the signals were comparable to those of *H2A.V* shRNA (Fig. 6I,L,M). As a control, levels of H2A.V were unaltered in somatic follicle cells, documenting the germline specificity of the effect (Fig. 6E-M). In remarkable contrast, loss of DOM-A or TIP60 did not affect levels of H2A.V (Fig. 6G,K-M). Likewise, depletion of ISWI ATPase, which causes similar germline phenotypes (Ables and Drummond-Barbosa, 2010; Xi and Xie, 2005; Yan et al., 2014), did not affect H2A.V levels (Fig. 6J,L,M). We conclude that DOM-B, but not DOM-A, is required for global incorporation of H2A.V into germline chromatin of the germarium.

Development (2016) 143, 3154-3167 doi:10.1242/dev.139634

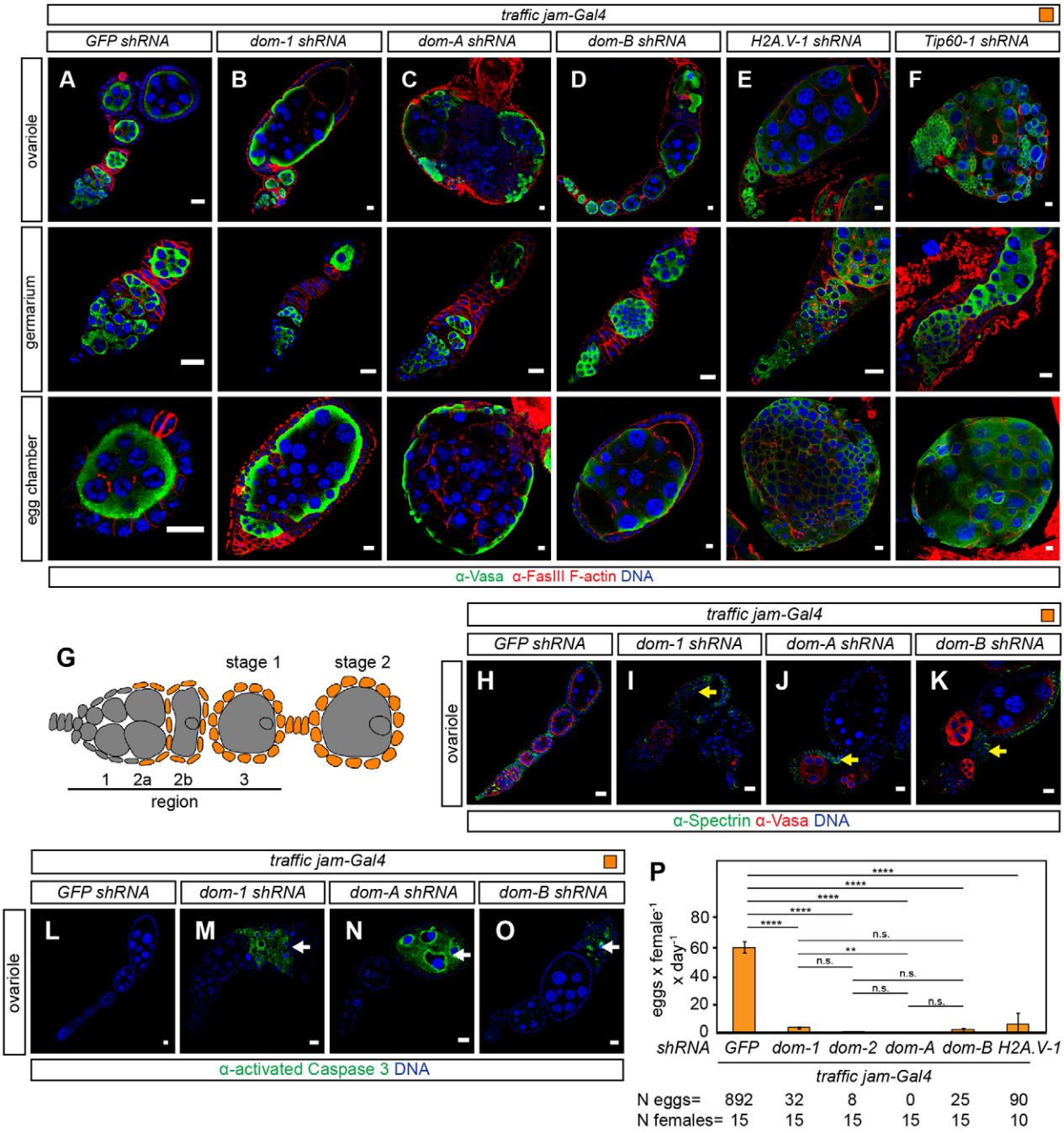

Fig. 5. Loss of DOM-A or DOM-B in somatic follicle cells leads to severe packaging defects. (A-F) Immunofluorescence images of ovariole, germarium and egg chamber with staining of Vasa (green), Fasciclin III and F-actin (red) and DNA (blue) for the following genotypes: *traffic jam-Gal4* with (A) *GFP*, (B) *dom-1*, (C) *dom-A*, (D) *dom-B*, (E) *H2A.V-1* and (F) *Tip60-1* shRNA. (G) Diagram of the early stages of *D. melanogaster* oogenesis. The specific expression pattern of the *traffic jam-Gal4* driver in somatic follicle cells is highlighted in orange. (H-K) Immunofluorescence images of ovarioles with staining of Spectrin (green), Vasa (red) and DNA (blue) for the following genotypes: *traffic jam-Gal4* with (H) *GFP*, (I) *dom-1*, (J) *dom-A* and (K) *dom-B* shRNA. Arrows indicate stalk-like structures. (L-O) Immunofluorescence images of ovarioles with staining of activated Caspase 3 (green) and DNA (blue) for the following genotypes: *traffic jam-Gal4* with (L) *GFP*, (M) *dom-1*, (N) *dom-A* and (O) *dom-B* shRNA. Arrows indicate apoptotic egg chambers. (P) Quantification of egg laying capacity. The data show mean values of eggs laid per female per day with s.d. of three biological replicates. *N* eggs represents the total number of scored eggs and *N* females the total number of analyzed females. ***P*<0.01, *****P*<0.0001; n.s., not significant. Two-tailed Student's *t*-test. Scale bars: 10 µm.

DOM-independent H2A.V incorporation in germline nurse cells

To monitor H2A.V levels in germline cells outside of the germarium we again employed the *matα4-Gal4* driver, which is specifically expressed from stage 1 of oogenesis onwards (Fig. 4A and Fig. S6) (Yan et al., 2014). As expected, *matα4-Gal4*-directed knockdown of DOM, DOM-A and DOM-B did not affect H2A.V levels in the germarium (Figs S7, S8). As a control, *H2A.V* shRNA knockdown specifically depleted H2A.V and γH2A.V in germline nurse cells of stage 3 egg chambers (Fig. 7A,E,G). Surprisingly, however, H2A.V and γH2A.V were unaltered in germline nurse cells up to stage 4 egg chambers upon DOM, DOM-A, DOM-B or TIP60 knockdown (Fig. 7B-D,F,G and Figs S7, S8). Notably,

Development (2016) 143, 3154-3167 doi:10.1242/dev.139634

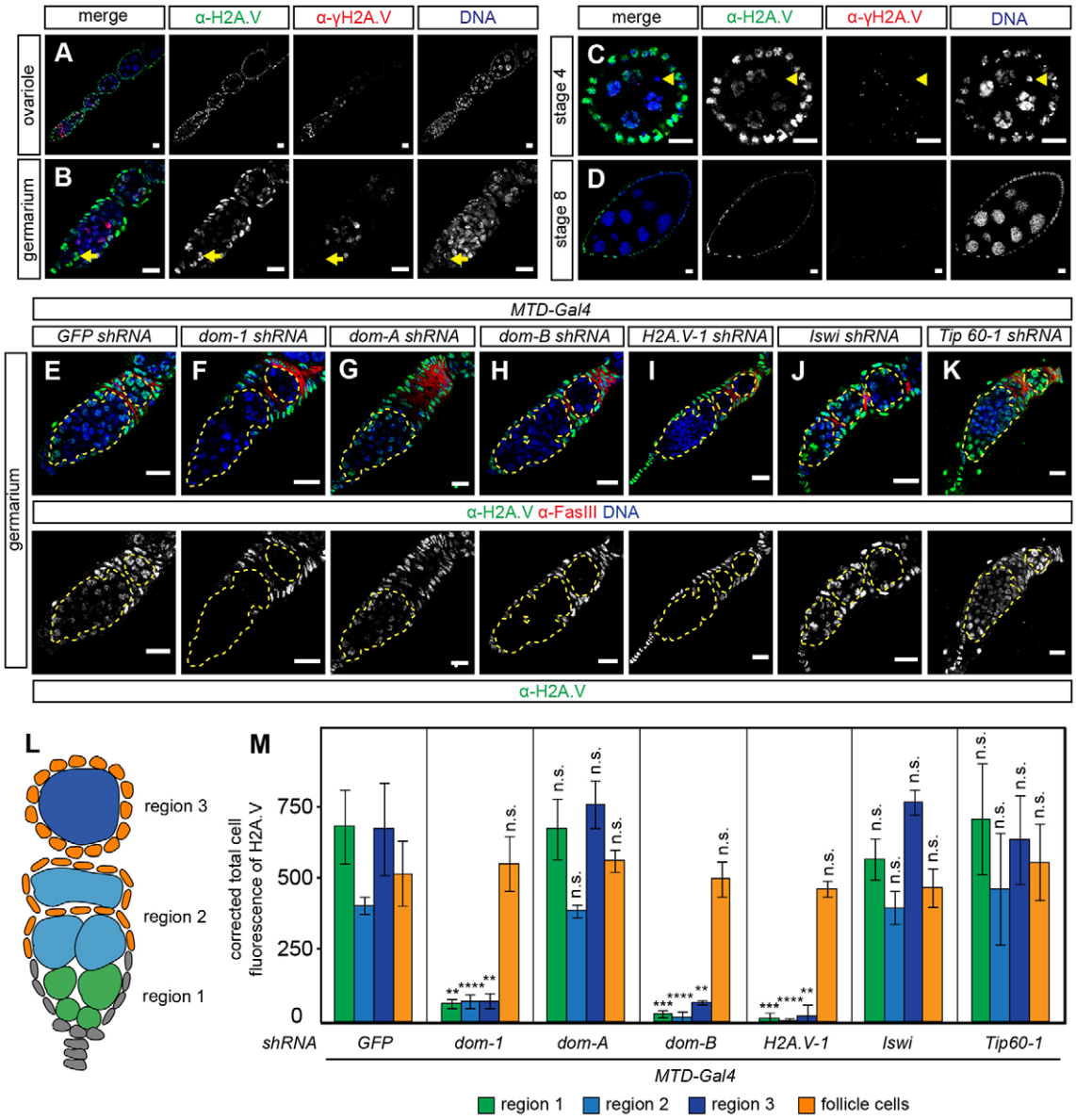

Fig. 6. DOM-B promotes global H2A.V incorporation into germline chromatin of the germarium. (A-D) Immunofluorescence images of ovariole, germarium, stage 4 and stage 8 egg chambers with staining of H2A.V (green), γH2A.V (red) and DNA (blue) for wild type. Arrows and arrowheads indicate GSCs and oocytes, respectively. (E-K) Immunofluorescence images of ovariole with staining of H2A.V (green), Fasciclin III (red) and DNA (blue) for the following genotypes: *MTD-Gal4* with (E) *GFP*, (F) *dom-1*, (G) *dom-A*, (H) *dom-B*, (I) *H2A.V-1*, (J) *Iswi* and (K) *Tip60-1* shRNA. Yellow dashed line indicates germline cells. (L) Diagram of *D. melanogaster* germarium. Green, light and dark blue indicate region 1, 2 and 3 of the germarium, respectively, as used for H2A.V signal quantification in M. (M) Quantification of H2A.V signals in germline and somatic cells of the germarium. Corrected total cell fluorescence of H2A.V was calculated for 30 germline cysts in different regions of the germarium and follicle cells, respectively. Mean values with s.d. of three biological replicates are shown. ***P*<0.01, ****P*<0.001, *****P*<0.0001; n.s., not significant. Two-tailed Student's *t*-test for comparison with *GFP* shRNA. Scale bars: 10 µm.

corresponding depletion of another SWI/SNF remodeler, INO80, with two different *Ino80* shRNAs (Bhatia et al., 2010; Yan et al., 2014) did not affect H2A.V localization in ovarioles (Fig. S9). This suggests that global H2A.V incorporation into germline chromatin at stage 3 might be independent of DOM.

Involvement of DOM-A/TIP60 in H2A.V eviction in germline cells from stage 5 onwards

We next assessed how depletion of individual DOM isoforms affects global H2A.V and γH2A.V in nurse cells of later egg chamber stages. Remarkably, H2A.V and γH2A.V signals persisted in stage 8 egg chambers upon DOM or DOM-A depletion (Fig. 8B,C,H,I,M and Figs S7, S8). Additionally, a moderate but significant increase of H2A.V as well as γH2A.V foci was detected upon TIP60 depletion (Fig. 8F,L,M). By contrast, H2A.V was removed in the absence of DOM-B as in wild-type ovarioles (Fig. 8A,D,G,J,M and Figs S7, S8). Evidently, DOM-A/TIP60 are specifically involved in removing H2A.V from germline cells by stage 5 of oogenesis, illustrating once more the functional diversification of the two splice variants.

DOM-B promotes global H2A.V incorporation into dividing follicle cell chromatin

To address whether other cell types also utilize DOM for H2A.V incorporation, we used the somatic driver *traffic jam-Gal4* for knockdown in follicle cells. As in germline cells of the germarium,

Development (2016) 143, 3154-3167 doi:10.1242/dev.139634

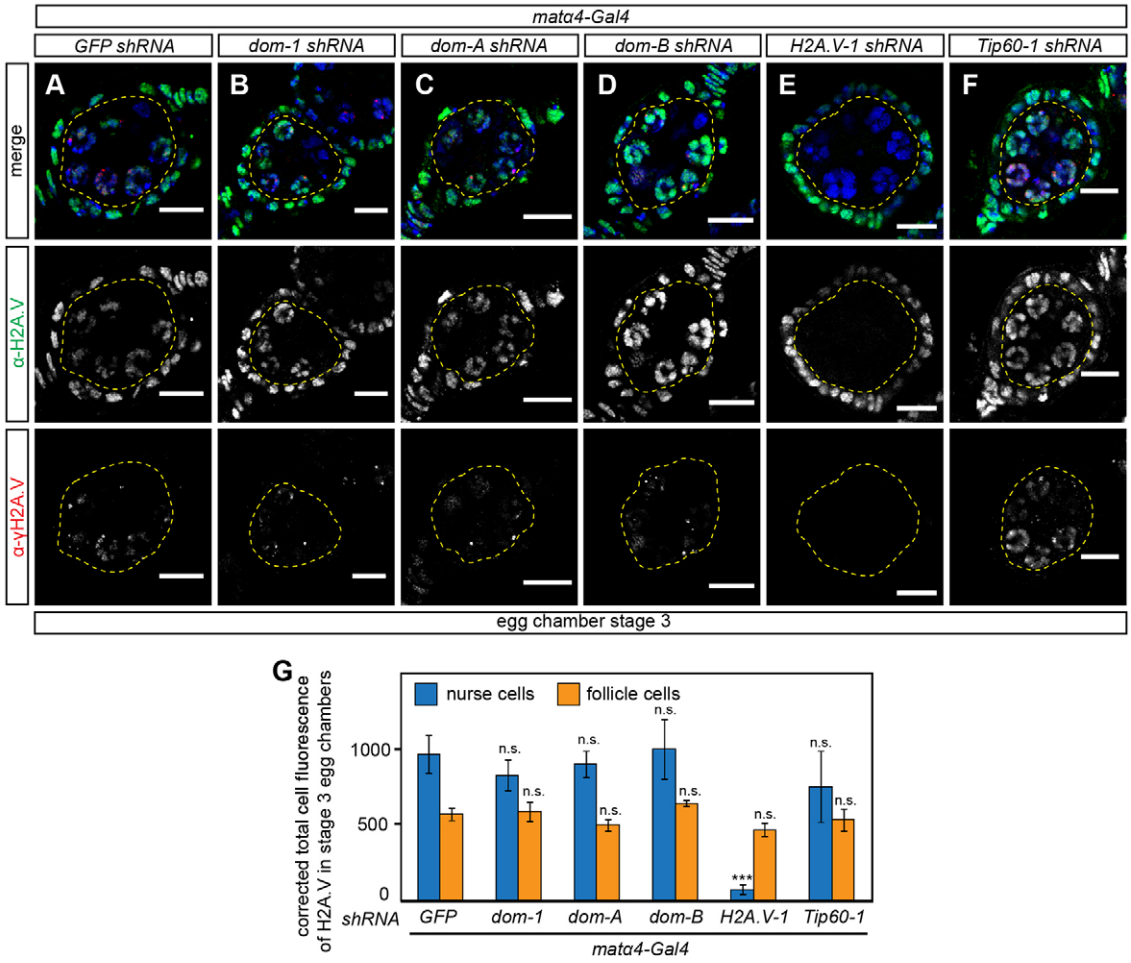

Fig. 7. DOM-independent H2A.V incorporation in germline nurse cells. (A-F) Immunofluorescence images of egg chambers with staining of H2A.V (green), γH2A.V (red) and DNA (blue) for the following genotypes: *matα4-Gal4* with (A) *GFP*, (B) *dom-1*, (C) *dom-A*, (D) *dom-B*, (E) *H2A.V-1* and (F) *Tip60-1* shRNA. Yellow dashed line indicates germline nurse cells. Scale bars: 10 µm. (G) Quantification of H2A.V signals in nurse and follicle cells of stage 3 egg chambers. Corrected total cell fluorescence of H2A.V was calculated for 50 germline nurse cells and 50 somatic follicle cells. Mean values with s.d. of three biological replicates are shown. ***P<0.001; n.s., not significant. Two-tailed Student's *t*-test for comparison with *GFP* shRNA.

we observed that depletion of DOM and DOM-B led to complete absence of H2A.V signals in follicle cell nuclei (Fig. 9A,B,D,H,I), when compared with the corresponding H2A.V knockdown (Fig. 9E,H,I). As before, *dom-A* and *Tip60* shRNAs did not affect H2A.V levels in follicle cells (Fig. 9C,G,H,I) and neither did depletion of ISWI (Fig. 9F,H,I), which causes similar packaging phenotypes (Börner et al., 2016). Furthermore, canonical histone H2A (Fig. 9J,K) and heterochromatin-associated HP1 protein (Fig. 9L,M) were unaltered upon DOM depletion, indicating a globally intact chromatin structure in the absence of H2A.V. This finding highlights the specific requirement of the DOM-B isoform for H2A.V incorporation not only in the germline but also in dividing somatic follicle cells.

In summary, our systematic analysis showed that the nucleosome remodeling factor isoforms DOM-A and DOM-B have non-redundant functions in germline and soma in the formation of egg chambers. We further demonstrated that the two DOM isoforms have distinct functions in H2A.V exchange during *D. melanogaster* oogenesis.

DISCUSSION

In *D. melanogaster* the properties of the two ancient, ubiquitous histone H2A variants H2A.X and H2A.Z are combined in a single molecule, H2A.V (Baldi and Becker, 2013; Talbert and Henikoff, 2010). Given that H2A.V carries out functions as a DNA damage sensor and architectural element of active promoters (Madigan et al., 2002; Mavrich et al., 2008), as well as having further roles in heterochromatin formation (Chioda et al., 2010; Hanai et al., 2008; Qi et al., 2006), this histone appears loaded with regulatory potential. Accordingly, placement of the variant, either randomly along with canonical H2A during replication or more specifically through nucleosome remodeling factors, becomes a crucial determinant in its function. Mechanistic detail for replacement of H2A-H2B dimers with variants comes from the analysis of the yeast SWR1 complex, which incorporates H2A.Z in a stepwise manner at strategic positions next to promoters (Luk et al., 2010; Mizuguchi et al., 2004; Ranjan et al., 2013).

So far, the published phenotypes associated with *dom* mutant alleles have not been systematically complemented (Braun et al., 1997; Eissenberg et al., 2005; Ruhf et al., 2001). Our comprehensive complementation analysis shows that *dom* mutant phenotypes are indeed due to defects in the *dom* gene. Remarkably, *dom* lethality and sterility can be partially rescued by complementation with the orthologous human *SRCAP* gene, providing an impressive example of functional conservation of SWR1-like remodelers (Eissenberg et al., 2005). The contributions of the two splice variants DOM-A

Development (2016) 143, 3154-3167 doi:10.1242/dev.139634

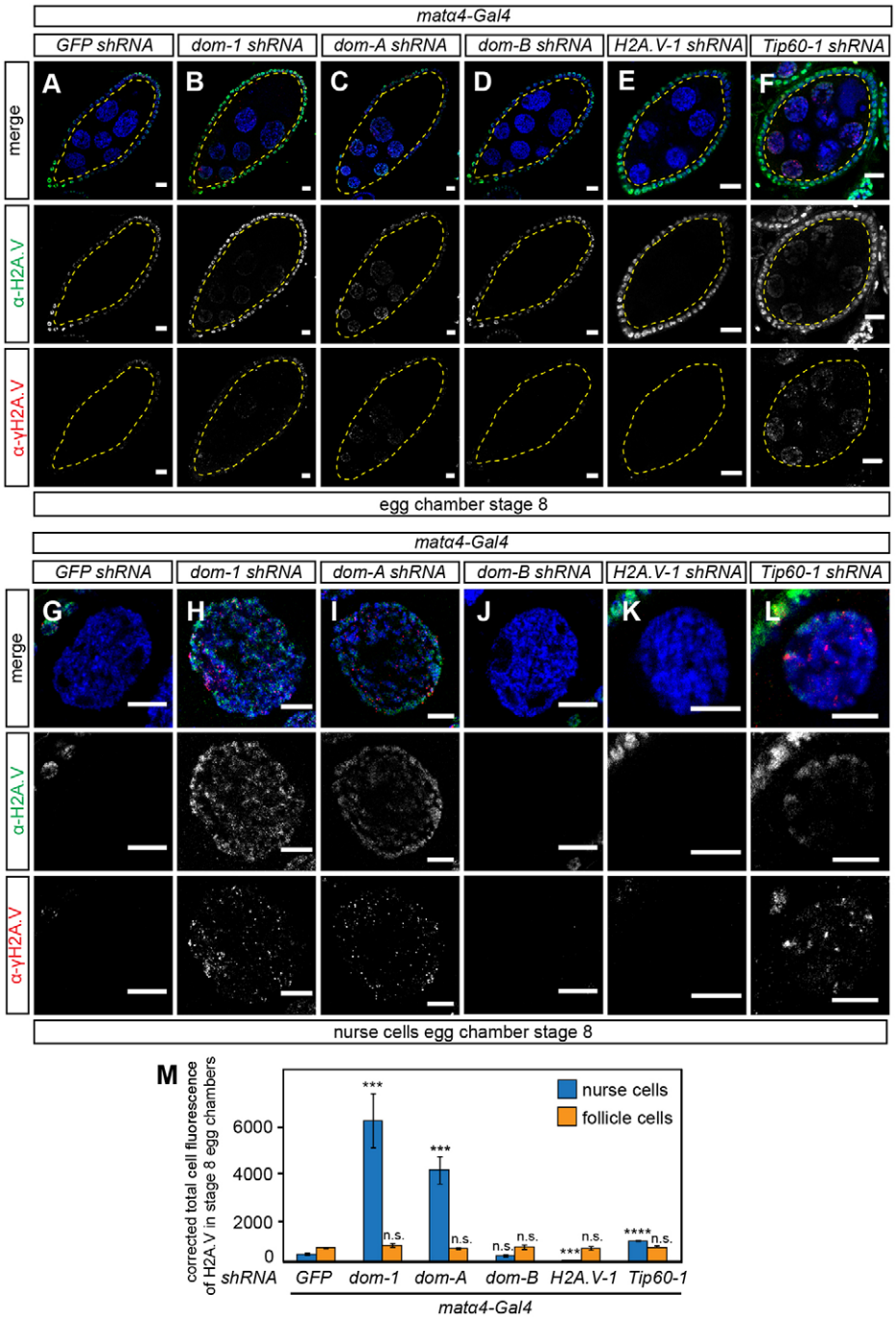

Fig. 8. Involvement of DOM-A/TIP60 in H2A.V eviction in germline cells from stage 5 onwards. (A-L) Immunofluorescence images of stage 8 egg chambers and nurse cells with staining of H2A.V (green), γH2A.V (red) and DNA (blue) for the following genotypes: *matα4-Gal4* with (A,G) *GFP*, (B,H) *dom-1*, (C,I) *dom-A*, (D,J) *dom-B*, (E,K) *H2A.V-1* and (F,L) *Tip60-1* shRNA. Yellow dashed line indicates germline nurse cells. Scale bars: 10 µm.
(M) Quantification of H2A.V persistence in germline nurse cells of stage 8 egg chambers. Corrected total cell fluorescence of H2A.V was calculated for 50 germline nurse cells and 50 somatic follicle cells. Mean values with s.d. of three biological replicates are shown. ***P<0.001, ****P<0.0001; n.s., not significant. Two-tailed Student's t-test for comparison with *GFP* shRNA.

and DOM-B had not been assessed. We now demonstrate that both isoforms are essential for development, suggesting non-redundant functions. The DOM-A isoform contains a SANT domain followed by several poly-Q stretches, which are widely found in transcriptional regulators, where they may modulate protein interactions (Gemayel et al., 2015). By contrast, SANT domains are thought to function as histone tail interaction modules that couple binding to enzyme catalysis (Boyer et al., 2004). Therefore, the SANT domain in DOM-A could mediate specificity towards H2A.V eviction depending on particular functional contexts. These features are also present in the C-terminus of p400 (EP400), the second human SWR1 ortholog, but are absent in either DOM-B or SRCAP (Eissenberg et al., 2005). Remarkably, p400 interacts directly with TIP60 (Jha et al., 2013) and the SANT domain of p400 inhibits TIP60 catalytic activity (Park et al., 2010), providing an interesting lead for further investigation of DOM isoforms and TIP60 interactions.

We speculate that distinct functions of p400 and SRCAP in humans might be accommodated to some extent by the two DOM isoforms in flies. Accordingly, it will be interesting to explore whether the two isoforms reside in distinct complexes. Previous affinity purification of a TIP60-containing complex using a tagged pontin subunit apparently only identified DOM-A, but not DOM-B (Kusch et al., 2004). Following up on the initial observation of early defects in GSCs and cyst differentiation upon loss of DOM (Yan et al., 2014), we now find that this phenotype is exclusively caused by loss of DOM-A. Interestingly, studies with human embryonic stem cells show that p400/TIP60 (KAT5) integrates pluripotency

Development (2016) 143, 3154-3167 doi:10.1242/dev.139634

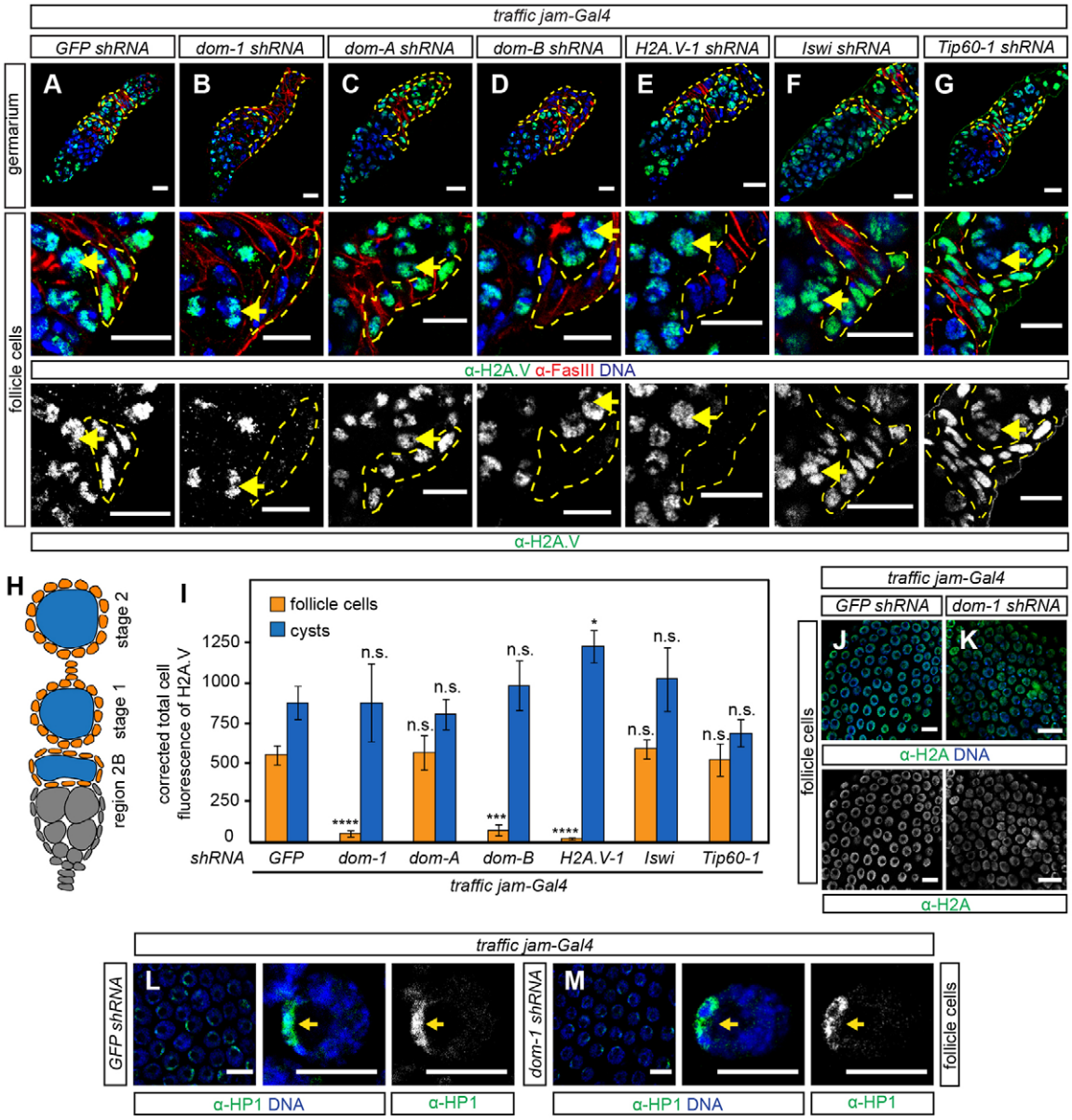

Fig. 9. DOM-B promotes global H2A.V incorporation into somatic follicle cell chromatin. (A-G) Immunofluorescence images of germarium with staining of H2A.V (green), Fasciclin III and F-actin (red) and DNA (blue) for the following genotypes: *traffic jam-Gal4* with (A) *GFP*, (B) *dom-1*, (C) *dom-A*, (D) *dom-B*, (E) *H2A.V-1*, (F) *Iswi* and (G) *Tip60-1* shRNA. Yellow dashed line indicates somatic follicle cells. Arrows indicate germline cysts. (H) Diagram of the early stages of *D. melanogaster* oogenesis. Orange and blue indicate follicle cells and cysts, respectively, as used for H2A.V signal quantification in I. (I) Quantification of H2A.V signals in somatic and germline cells. Corrected total cell fluorescence of H2A.V was calculated for 30 somatic follicle cells and 30 cysts. Mean values with s.d. of three biological replicates are shown. **P*<0.05, ****P*<0.001, *****P*<0.0001; n.s., not significant. Two-tailed Student's *t*-test for comparison with *GFP* shRNA. (J,K) Immunofluorescence images of follicle cells with staining of H2A (green) and DNA (blue) for the following genotypes: *traffic jam-Gal4* with (J) *GFP* and (K) *dom-1* shRNA. (L,M) Immunofluorescence images of follicle cells with staining of HP1 (green) and DNA (blue) for the following genotypes: *traffic jam-Gal4* with (L) *GFP* and (M) *dom-1* shRNA. Arrows indicate heterochromatic domain. Scale bars: 10 µm.

signals to regulate gene expression (Chen et al., 2013; Fazzio et al., 2008), suggesting similar roles for DOM-A in GSCs. This is in contrast to requirements for both isoforms for germline development outside of the germarium, highlighting a developmental specialization of the two DOM remodelers.

DOM is also involved in the differentiation and function of SSCs in the germarium (Xi and Xie, 2005). Our data now document non-redundant requirements of both DOM isoforms in somatic cells for proper coordination of follicle cell proliferation with cyst differentiation. Failure to adjust these two processes leads to 16-cell cyst packaging defects that manifest as compound egg chambers. These rare phenotypes had previously only been described upon perturbation of some signaling pathways, such as Notch, or Polycomb regulation (Jackson and Blochlinger, 1997; Narbonne et al., 2004).

Because the phenotypes of DOM depletions resemble those of H2A.V depletion we favor the idea that many of the cell-specification defects are due to compromised H2A.V incorporation, depriving key promoters of the H2A.Z-related architectural function. Alternatively, scaffolding activities might partially explain some roles of chromatin remodelers, as suggested for SRCAP (Bowman et al., 2011). So far, our knowledge of the

Development (2016) 143, 3154-3167 doi:10.1242/dev.139634

mechanisms of H2A.V incorporation has been anecdotal (Joyce et al., 2011; Kusch et al., 2014; Lu et al., 2007). Our comprehensive analysis revealed a specific involvement of DOM-B for the incorporation of H2A.V into chromatin at the global level. The N-termini of SWR1 and DOM-B harbor the HSA and ATPase spacer domains (Morrison and Shen, 2009), with interaction surfaces for further complex subunits (Billon and Côté, 2012; Gerhold and Gasser, 2014), and an additional H2A.Z-H2B dimer binding site (Wu et al., 2005, 2009). Given the requirement for both isoforms for cell specification during oogenesis, we speculate that DOM-B might serve to incorporate bulk H2A.V into chromatin similar to SWR1, whereas DOM-A would be more involved in the regulatory refinement of location.

Although the failures in cell specification and egg morphogenesis are likely to be explained by loss of the H2A.Z-related features of H2A.V, ablation of DOM might also compromise the DNA damage response, which involves phosphorylation of H2A.V (γH2A.V). Conceivably, the role of γH2A.V as a DNA damage sensor might be best fulfilled by a broad distribution of H2A.V throughout the chromatin (Baldi and Becker, 2013). Such an untargeted incorporation may be achieved by stochastic, chaperone-mediated incorporation during replication (Li et al., 2012) or by an untargeted activity of DOM-B. We observed DOM-independent incorporation in endoreplicating polyploid nurse cells of stage 3 egg chambers, where global H2A.V and γH2A.V signals did not depend on DOM. Immunofluorescence microscopy may lack the sensitivity to detect DOM-dependent incorporation of H2A.V at some specific sites. Nevertheless, DOM-independent incorporation of H2A.V might serve to cope with many naturally occurring DNA double-strand breaks during the massive endoreplication of nurse cells.

There is some evidence that nucleosome remodelers not only incorporate H2A variants but can also remove them. In yeast, the genome-wide distribution of H2A.Z appears to be established by the antagonistic functions of the SWR1 and Ino80 remodeling complexes, where Ino80 replaces stray H2A.Z-H2B with canonical H2A-H2B dimers (Papamichos-Chronakis et al., 2011). A recent study identified the vertebrate-specific histone chaperone ANP32E as part of a TIP60/p400 complex that facilitates the eviction of H2A.Z-H2B dimers from chromatin (Obri et al., 2014). Remarkably, in *D. melanogaster* a TIP60/DOM-A complex is involved in a similar reaction. The TIP60/DOM-A complex acetylates γH2A.V at lysine 5 to facilitate exchange of γH2A.V by unmodified H2A.V during the DNA damage response (Kusch et al., 2004). Furthermore, it has been speculated that H2A.V and γH2A.V could be actively removed from nurse cells, since corresponding signals are absent from stage 5 onwards (Jang et al., 2003; Joyce et al., 2011). We now demonstrate that depletion of DOM-A and TIP60 leads to the persistence of H2A.V and γH2A.V in nurse cells of late egg chambers, clearly documenting the ability of the remodeler to remove bulk H2A.V and variants modified during DNA damage induction.

Our findings highlight the specific requirements of DOM splice variants for the incorporation and removal of H2A.V during *D. melanogaster* oogenesis. It remains an interesting and challenging question how DOM-A and DOM-B complexes are targeted genome-wide and function *in vivo* to establish specific H2A.V patterns in different cell types during development.

MATERIALS AND METHODS

D. melanogaster strains and genetics

The genomic region of *dom* was modified by recombineering in *Escherichia coli* using pRedFLP4 recombination technology (Ejsmont et al., 2009). Details are provided in the supplementary Materials and Methods and in Tables S1 and S2. All fosmid, *UAS-shRNA* and *Gal4* driver lines are listed in the supplementary Materials and Methods. For ovary analysis, *UAS-shRNA* males were crossed with *Gal4* driver virgins at 29°C and 5- to 7-day-old F1 females were used, unless stated otherwise.

Complementation assays

Males and female virgins of dom^{1}/*bcg*; *dom* fosmid/+ or of dom^{9}/*bcg*; *dom* fosmid/+ genotype were crossed. F1 offspring were analyzed for *bcg* phenotype and rescue of pupal lethality was determined as percentage of observed to expected frequency of homozygous dom^{1} or dom^{9} offspring. Mean values in percentage with s.d. from three biological replicates were calculated.

Necrotic lymph glands were scored in third instar larvae of homozygous w^{1118}, dom^{1}, dom^{1};*GFP-dom*, dom^{1};*dom-A-GFP* and dom^{1};*dom-B-GFP*. Mean values in percentage with s.d. from three biological replicates were calculated.

Homozygous female virgins for w^{1118}, dom^{9}, dom^{9};*GFP-dom*, dom^{9};*dom-A-GFP*, dom^{9};*dom-B-GFP* and dom^{9};Δ*dom-GFP* were collected for 2-3 days at 25°C. Females of each genotype were mated with w^{1118} males in vials with yeast paste for 2 days. Females were placed in individual vials for 3 days without males and the egg laying capacity determined as the number of eggs laid per female per day. The data were averaged and mean values with s.d. from three biological replicates calculated.

Pupal hatching assay

UAS-shRNA males for *GFP*, *dom-1*, *dom-A* and *dom-B* were crossed with *actin-Gal4*/*CyO* driver virgins at 25°C. Pupae were transferred to new vials and numbered. A 1:1 ratio of *CyO* and *actin-Gal4* F1 siblings was expected. *CyO* phenotype was counted and pupal hatching was determined as the observed to expected frequency of *CyO* and *actin-Gal4* F1 siblings. Mean values in percentage with s.d. from three biological replicates were calculated.

Egg laying assay

Homozygous *UAS-shRNA* males for *GFP*, *dom-1*, *dom-2*, *dom-A* and *dom-B* were crossed with *MTD-*, *matα4-*, *c587-* or *traffic jam-Gal4* driver virgins at 29°C. F1 female virgins of each genotype (2-3 days old) were mated with w^{1118} males in vials with yeast paste for 2 days. Females were then placed in individual vials without males and the egg laying capacity determined as described above.

Analysis of wing phenotypes

UAS-shRNA males for *GFP*, *dom-1*, *dom-2*, *dom-A* and *dom-B* were crossed with *C96-Gal4* driver virgins at 29°C. Wing phenotypes were scored in F1 offspring and relative mean values in percentages with s.d. from three biological replicates were calculated.

Generation of DOA1, DOB2 and H2A.V antibodies

DOA1, DOB2 and H2A.V antibodies were made for this study as described in the supplementary Materials and Methods.

Immunological techniques and microscopy

Immunofluorescence microscopy was performed using standard procedures and a Leica TCS SP5 II confocal microscope. Images were processed using ImageJ (NIH) and Adobe Photoshop. For details, including the antibodies used, see the supplementary Materials and Methods.

Western blot

Twelve pairs of ovaries or 20 brains of third instar larvae were dissected, homogenized in Laemmli buffer and incubated at 95°C for 5 min. Western blot was performed using standard procedures; antibodies are listed in the supplementary Materials and Methods.

Statistical test

Two-tailed Student's *t*-test was used. *P*-values are given in the figure legends.

Acknowledgements
Some stocks were obtained from the Bloomington Drosophila Stock Center [NIH P40OD018537]. We thank the TRiP at Harvard Medical School [NIH/NIGMS R01-GM084947] for transgenic RNAi fly lines. The monoclonal antibodies ORB 4H8 and 6H4, 7G10 anti-Fasciclin III, Spectrin 3A9 (323 or M10-2), HP1 C1A9 and UNC93-5.2.1 were obtained from the Developmental Studies Hybridoma Bank. We thank A. Eberharter, J.-R. Huynh, J. Jiang, E. Kremmer, J. Müller, H. Saumweber, A. Spradling and P. Tomancak for providing reagents; and S. Baldi, D. Jain, N. Steffen and S. Vengadasalam for stimulating discussions.

Competing interests
The authors declare no competing or financial interests.

Author contributions
K.B. performed experiments; K.B. and P.B.B. developed concepts and approaches, analyzed data and prepared the manuscript.

Funding
This work was supported by the Deutsche Forschungsgemeinschaft [grants Be1140/7-1 and SFB1064/A01].

Supplementary information
Supplementary information available online at
http://dev.biologists.org/lookup/doi/10.1242/dev.139634.supplemental

References

Ables, E. T. and Drummond-Barbosa, D. (2010). The steroid hormone ecdysone functions with intrinsic chromatin remodeling factors to control female germline stem cells in Drosophila. *Cell Stem Cell* **7**, 581-592.
Baldi, S. and Becker, P. B. (2013). The variant histone H2A.V of Drosophila-three roles, two guises. *Chromosoma* **122**, 245-258.
Bhatia, S., Pawar, H., Dasari, V., Mishra, R. K., Chandrashekaran, S. and Brahmachari, V. (2010). Chromatin remodeling protein INO80 has a role in regulation of homeotic gene expression in Drosophila. *Genes Cells* **15**, 725-735.
Billon, P. and Côté, J. (2012). Precise deposition of histone H2A.Z in chromatin for genome expression and maintenance. *Biochim. Biophys. Acta-Gene Regul. Mech.* **1819**, 290-302.
Bönisch, C. and Hake, S. B. (2012). Histone H2A variants in nucleosomes and chromatin: more or less stable? *Nucleic Acids Res.* **40**, 10719-10741.
Börner, K., Jain, D., Vazquez-Pianzola, P., Vengadasalam, S., Steffen, N., Fyodorov, D. V., Tomancak, P., Konev, A., Suter, B. and Becker, P. B. (2016). A role for tuned levels of nucleosome remodeler subunit ACF1 during Drosophila oogenesis. *Dev. Biol.* **411**, 217-230.
Bowman, T. A., Wong, M. M., Cox, L. K., Baldassare, J. J. and Chrivia, J. C. (2011). Loss of H2A.Z is not sufficient to determine transcriptional activity of Snf2-related CBP activator protein or p400 complexes. *Int. J. Cell Biol.* **2011**, 715642.
Boyer, L. A., Latek, R. R. and Peterson, C. L. (2004). The SANT domain: a unique histone-tail-binding module? *Nat. Rev. Mol. Cell Biol.* **5**, 158-163.
Braun, A., Lemaitre, B., Lanot, R., Zachary, D. and Meister, M. (1997). Drosophila immunity: analysis of larval hemocytes by P-element-mediated enhancer trap. *Genetics* **147**, 623-634.
Braun, A., Hoffmann, J. A. and Meister, M. (1998). Analysis of the Drosophila host defense in domino mutant larvae, which are devoid of hemocytes. *Proc. Natl. Acad. Sci. USA* **95**, 14337-14342.
Cai, Y., Jin, J., Florens, L., Swanson, S. K., Kusch, T., Li, B., Workman, J. L., Washburn, M. P., Conaway, R. C. and Conaway, J. W. (2005). The mammalian YL1 protein is a shared subunit of the TRRAP/TIP60 histone acetyltransferase and SRCAP complexes. *J. Biol. Chem.* **280**, 13665-13670.
Chen, P. B., Hung, J.-H., Hickman, T. L., Coles, A. H., Carey, J. F., Weng, Z., Chu, F. and Fazzio, T. G. (2013). Hdac6 regulates Tip60-p400 function in stem cells. *Elife* **2**, e01557.
Chioda, M. and Becker, P. B. (2010). Soft skills turned into hard facts: nucleosome remodelling at developmental switches. *Heredity* **105**, 71-79.
Chioda, M., Vengadasalam, S., Kremmer, E., Eberharter, A. and Becker, P. B. (2010). Developmental role for ACF1-containing nucleosome remodellers in chromatin organisation. *Development* **137**, 3513-3522.
Eissenberg, J. C., Wong, M. and Chrivia, J. C. (2005). Human SRCAP and Drosophila melanogaster DOM are homologs that function in the notch signaling pathway. *Mol. Cell. Biol.* **25**, 6559-6569.
Eliazer, S., Shalaby, N. A. and Buszczak, M. (2011). Loss of lysine-specific demethylase 1 nonautonomously causes stem cell tumors in the Drosophila ovary. *Proc. Natl. Acad. Sci. USA* **108**, 7064-7069.
Ellis, K., Friedman, C. and Yedvobnick, B. (2015). Drosophila domino exhibits genetic interactions with a wide spectrum of chromatin protein-encoding loci. *PLoS ONE* **10**, e0142635.
Ejsmont, R. K., Sarov, M., Winkler, S., Lipinski, K. A. and Tomancak, P. (2009). A toolkit for high-throughput, cross-species gene engineering in Drosophila. *Nat. Methods* **6**, 435-437. .
Fazzio, T. G., Huff, J. T. and Panning, B. (2008). An RNAi screen of chromatin proteins identifies Tip60-p400 as a regulator of embryonic stem cell identity. *Cell* **134**, 162-174.
Gause, M., Eissenberg, J. C., Macrae, A. F., Dorsett, M., Misulovin, Z. and Dorsett, D. (2006). Nipped-A, the Tra1/TRRAP subunit of the Drosophila SAGA and Tip60 complexes, has multiple roles in notch signaling during wing development. *Mol. Cell. Biol.* **26**, 2347-2359.
Gemayel, R., Chavali, S., Pougach, K., Legendre, M., Zhu, B., Boeynaems, S., van der Zande, E., Gevaert, K., Rousseau, F., Schymkowitz, J. et al. (2015). Variable glutamine-rich repeats modulate transcription factor activity. *Mol. Cell* **59**, 615-627.
Gerhold, C. B. and Gasser, S. M. (2014). INO80 and SWR complexes: relating structure to function in chromatin remodeling. *Trends Cell Biol.* **24**, 1-13.
Hanai, K., Furuhashi, H., Yamamoto, T., Akasaka, K. and Hirose, S. (2008). RSF governs silent chromatin formation via histone H2Av replacement. *PLoS Genet.* **4**, e1000011.
Ho, L. and Crabtree, G. R. (2010). Chromatin remodelling during development. *Nature* **463**, 474-484.
Hudson, A. M. and Cooley, L. (2014). Methods for studying oogenesis. *Methods* **68**, 207-217.
Iovino, N. (2014). Drosophila epigenome reorganization during oocyte differentiation and early embryogenesis. *Brief. Funct. Genomics* **13**, 246-253.
Jackson, S. M. and Blochlinger, K. (1997). cut interacts with Notch and protein kinase A to regulate egg chamber formation and to maintain germline cyst integrity during Drosophila oogenesis. *Development* **124**, 3663-3672.
Jang, J. K., Sherizen, D. E., Bhagat, R., Manheim, E. A. and Mckim, K. S. (2003). Relationship of DNA double-strand breaks to synapsis in Drosophila. *J. Cell Sci.* **116**, 3069-3077.
Jha, S., Gupta, A., Dar, A. and Dutta, A. (2013). RVBs are required for assembling a functional TIP60 complex. *Mol. Cell. Biol.* **33**, 1164-1174.
Jin, J., Cai, Y., Li, B., Conaway, R. C., Workman, J. L., Conaway, J. W. and Kusch, T. (2005). In and out: histone variant exchange in chromatin. *Trends Biochem. Sci.* **30**, 680-687.
Joyce, E. F., Pedersen, M., Tiong, S., White-Brown, S. K., Paul, A., Campbell, S. D. and McKim, K. S. (2011). Drosophila ATM and ATR have distinct activities in the regulation of meiotic DNA damage and repair. *J. Cell Biol.* **195**, 359-367.
Kai, T. and Spradling, A. (2003). An empty Drosophila stem cell niche reactivates the proliferation of ectopic cells. *Proc. Natl. Acad. Sci. USA* **100**, 4633-4638.
Kusch, T., Florens, L., MacDonald, W. H., Swanson, S. K., Glaser, R. L., Yates, J. R., Abmayr, S. M., Washburn, M. P. and Workman, J. L. (2004). Acetylation by Tip60 is required for selective histone variant exchange at DNA lesions. *Science* **306**, 2084-2087.
Kusch, T., Mei, A. and Nguyen, C. (2014). Histone H3 lysine 4 trimethylation regulates cotranscriptional H2A variant exchange by Tip60 complexes to maximize gene expression. *Proc. Natl. Acad. Sci. USA* **111**, 4850-4855.
Kwon, M. H., Callaway, H., Zhong, J. and Yedvobnick, B. (2013). A targeted genetic modifier screen links the SWI2/SNF2 protein domino to growth and autophagy genes in Drosophila melanogaster. *G3* **3**, 815-825.
Li, Z., Thiel, K., Thul, P. J., Beller, M., Kühnlein, R. P. and Welte, M. A. (2012). Lipid droplets control the maternal histone supply of Drosophila embryos. *Curr. Biol.* **22**, 2104-2113.
Lu, J., Ruhf, M.-L., Perrimon, N. and Leder, P. (2007). A genome-wide RNA interference screen identifies putative chromatin regulators essential for E2F repression. *Proc. Natl. Acad. Sci. USA* **104**, 9381-9386.
Luk, E., Ranjan, A., FitzGerald, P. C., Mizuguchi, G., Huang, Y., Wei, D. and Wu, C. (2010). Stepwise histone replacement by SWR1 requires dual activation with histone H2A.Z and canonical nucleosome. *Cell* **143**, 725-736.
Madigan, J. P., Chotkowski, H. L. and Glaser, R. L. (2002). DNA double-strand break-induced phosphorylation of Drosophila histone variant H2Av helps prevent radiation-induced apoptosis. *Nucleic Acids Res.* **30**, 3698-3705.
Mavrich, T. N., Jiang, C., Ioshikhes, I. P., Li, X., Venters, B. J., Zanton, S. J., Tomsho, L. P., Qi, J., Glaser, R. L., Schuster, S. C. et al. (2008). Nucleosome organization in the Drosophila genome. *Nature* **453**, 358-362.
Messina, G., Damia, E., Fanti, L., Atterrato, M. T., Celauro, E., Mariotti, F. R., Accardo, M. C., Walther, M., Vernì, F., Picchioni, D. et al. (2014). Yeti, an essential Drosophila melanogaster gene, encodes a protein required for chromatin organization. *J. Cell Sci.* **127**, 2577-2588.
Mizuguchi, G., Shen, X., Landry, J., Wu, W.-H., Sen, S. and Wu, C. (2004). ATP-driven exchange of histone H2AZ variant catalyzed by SWR1 chromatin remodeling complex. *Science* **303**, 343-348.
Morillo Prado, J. R., Srinivasan, S. and Fuller, M. T. (2013). The histone variant His2Av is required for adult stem cell maintenance in the Drosophila testis. *PLoS Genet.* **9**, e1003903.
Morrison, A. J. and Shen, X. (2009). Chromatin remodelling beyond transcription: the INO80 and SWR1 complexes. *Nat. Rev. Mol. Cell Biol.* **10**, 373-384.

Narbonne, K., Besse, F., Brissard-Zahraoui, J., Pret, A.-M. and Busson, D. (2004). polyhomeotic is required for somatic cell proliferation and differentiation during ovarian follicle formation in Drosophila. *Development* **131**, 1389-1400.
Ni, J.-Q., Zhou, R., Czech, B., Liu, L.-P., Holderbaum, L., Yang-Zhou, D., Shim, H.-S., Tao, R., Handler, D., Karpowicz, P. et al. (2011). A genome-scale shRNA resource for transgenic RNAi in Drosophila. *Nat. Methods* **8**, 405-407.
Obri, A., Ouararhni, K., Papin, C., Diebold, M.-L., Padmanabhan, K., Marek, M., Stoll, I., Roy, L., Reilly, P. T., Mak, T. W. et al. (2014). ANP32E is a histone chaperone that removes H2A.Z from chromatin. *Nature* **505**, 648-653.
Olivieri, D., Sykora, M. M., Sachidanandam, R., Mechtler, K. and Brennecke, J. (2010). An in vivo RNAi assay identifies major genetic and cellular requirements for primary piRNA biogenesis in Drosophila. *EMBO J.* **29**, 3301-3317.
Papamichos-Chronakis, M., Watanabe, S., Rando, O. J. and Peterson, C. L. (2011). Global regulation of H2A.Z localization by the INO80 chromatin-remodeling enzyme is essential for genome integrity. *Cell* **144**, 200-213.
Park, J. H., Sun, X.-J. and Roeder, R. G. (2010). The SANT domain of p400 ATPase represses acetyltransferase activity and coactivator function of TIP60 in basal p21 gene expression. *Mol. Cell. Biol.* **30**, 2750-2761.
Qi, D., Jin, H., Lilja, T. and Mannervik, M. (2006). Drosophila Reptin and other TIP60 complex components promote generation of silent chromatin. *Genetics* **174**, 241-251.
Ranjan, A., Mizuguchi, G., FitzGerald, P. C., Wei, D., Wang, F., Huang, Y., Luk, E., Woodcock, C. L. and Wu, C. (2013). Nucleosome-free region dominates histone acetylation in targeting SWR1 to promoters for H2A.Z replacement. *Cell* **154**, 1232-1245.
Ruhf, M. L., Braun, A., Papoulas, O., Tamkun, J. W., Randsholt, N. and Meister, M. (2001). The domino gene of Drosophila encodes novel members of the SWI2/SNF2 family of DNA-dependent ATPases, which contribute to the silencing of homeotic genes. *Development* **128**, 1429-1441.
Ruhl, D. D., Jin, J., Cai, Y., Swanson, S., Florens, L., Washburn, M. P., Conaway, R. C., Conaway, J. W. and Chrivia, J. C. (2006). Purification of a human SRCAP complex that remodels chromatin by incorporating the histone variant H2A.Z into nucleosomes. *Biochemistry* **45**, 5671-5677.
Sadasivam, D. A. and Huang, D.-H. (2016). Maintenance of tissue pluripotency by epigenetic factors acting at multiple levels. *PLOS Genet.* **12**, e1005897.
Talbert, P. B. and Henikoff, S. (2010). Histone variants–ancient wrap artists of the epigenome. *Nat. Rev. Mol. Cell Biol.* **11**, 264-275.
Ting, X. (2013). Control of germline stem cell self-renewal and differentiation in the Drosophila ovary: concerted actions of niche signals and intrinsic factors. *Wiley Interdiscip. Rev. Dev. Biol.* **2**, 261-273.
Walker, J., Kwon, S. Y., Badenhorst, P., East, P., McNeill, H. and Svejstrup, J. Q. (2011). Role of elongator subunit Elp3 in Drosophila melanogaster larval development and immunity. *Genetics* **187**, 1067-1075.
Wu, W.-H., Alami, S., Luk, E., Wu, C.-H., Sen, S., Mizuguchi, G., Wei, D. and Wu, C. (2005). Swc2 is a widely conserved H2AZ-binding module essential for ATP-dependent histone exchange. *Nat. Struct. Mol. Biol.* **12**, 1064-1071.
Wu, W.-H., Wu, C.-H., Ladurner, A., Mizuguchi, G., Wei, D., Xiao, H., Luk, E., Ranjant, A. and Wu, C. (2009). N terminus of Swr1 binds to histone H2AZ and provides a platform for subunit assembly in the chromatin remodeling complex. *J. Biol. Chem.* **284**, 6200-6207.
Xi, R. and Xie, T. (2005). Stem cell self-renewal controlled by chromatin remodeling factors. *Science* **310**, 1487-1489.
Yan, D., Neumüller, R. A., Buckner, M., Ayers, K., Li, H., Hu, Y., Yang-Zhou, D., Pan, L., Wang, X., Kelley, C. et al. (2014). A regulatory network of drosophila germline stem cell self-renewal. *Dev. Cell* **28**, 459-473.

Supplementary information

D. melanogaster strains and genetics

DOM-A and DOM-B protein sequences correspond to DOM-RA and DOM-RE transcripts, respectively (flybase.org, FB2016_03, released May 24, 2016). The *domino (dom)* fosmid derivatives are based on the fosmid library clone pflyfos016675 (kind gift of P. Tomancak, MPI-CPG, Germany). The *GFP-dom* fosmid codes for DOM with an N-terminal 2xTY1-sGFP-3xFLAG-tag which tags both isoforms DOM-A and DOM-B. The *dom-A-GFP* and *dom-B-GFP* fosmids code for DOM with a C-terminal 2xTY1-sGFP-3xFLAG-tag which tags DOM-A and DOM-B, respectively. The entire *dom* locus was replaced with 2xTY1-sGFP-3xFLAG-tag in the Δ*dom-GFP* fosmid. All oligonucleotide sequences and combinations are listed (Tabs. S1 and S2). All *dom* fosmid variants were verified by restriction enzyme digestion, PCR and sequencing before injection into *D. melanogaster*. Transgenic flies were made by phiC31 integrase-mediated site-specific integration into attP2 landing site on the 3rd chromosome (Genetic Services, Inc., USA). Fosmid constructs contain *dsRed* cassette driven by 3xP3 promoter to select for transformants.

The following homozygous fly lines containing fosmid constructs were obtained by appropriate crosses: *GFP-dom*, *dom-A-GFP*, *dom-B-GFP*, Δ*dom-GFP*, *dom*^{1};*GFP-dom*, *dom*^{1};*dom-A-GFP*, *dom*^{1};*dom-B-GFP*, *dom*^{9};*GFP-dom*, *dom*^{9};*dom-A-GFP*, *dom*^{9};*dom-B-GFP*, *dom*^{9};Δ*dom-GFP*, *traffic jam-Gal4*/*bcg*;*GFP-dom*, *traffic jam-Gal4*/*bcg*;*dom-A-GFP* and *traffic jam-Gal4*/*bcg*;*dom-B-GFP*.

UAS-shdom-A (HMC04451, attP2, Val20) and *UAS-shdom-B* (HMC04203, attP2, Val20) were made for this study by and *UAS-shdom-1* (HMS02612, attP2, Val20), *UAS-shdom-2* (HMS01855, attP2, Val20), *UAS-shH2A.V-1* (HM05177, attP2, Val10), *UAS-shH2A.V-2* (HMS00162, attP2, Val20), *UAS-shIno80.1* (HMS00586, attP2, Val20), *UAS-shIno80.2* (GL00616, attP2, Val22), *UAS-shIswi* (HMS00628, attP40, Val20), *UAS-shTip60-1* (HM05049, attP2, Val10) and *UAS-shTip60-2* (GL00130, attP2, Val22) were obtained from Transgenic RNAi Project (TRiP, Harvard Medical School, Boston, USA). *UAS-shEGFP* (#41557, attP40, Val22), *MTD-Gal4* (#31777), *matα4-Gal4* (#7063), *actin-Gal4*/*CyO* (#25708), *elav-Gal4* (#25750), *C96-Gal4* (#25757), *dom*^{1} (#10767) and *dom*^{9} (#9261) were obtained from Bloomington Drosophila Stock Center (BDSC, USA). *c587-Gal4* and *traffic jam-Gal4* were kind gifts of Allan C. Spradling (Carnegie Institution for Science, USA) and Jean-René Huynh (Institut Curie, France), respectively.

Generation of DOA1, DOB2 and H2A.V antibodies

DOA1 (KEHKRSRTDAGYDGSRRPNC) and DOB2 (TPKESQSEPRRKITQPKC) peptides with N-terminal PEG-Biotin and C-terminal coupled Ovalbumin were made by Peptide Specialty Laboratories (PSL, Germany). The monoclonal rat DOA1 17F4 and mouse DOB2 4H4 peptide antibodies were developed by E. Kremmer (Helmholtz Zentrum Munich, Germany). The specificity was confirmed in Western blot by RNAi (Fig. 2B) and with recombinantly expressed, C-terminally tagged DOM-A and

DOM-B (data not shown). Some lower-molecular weight bands were only detected with DOA1 but not with FLAG antibody suggesting limited degradation (data not shown).

H2A.V peptide (QPDQRKGNVIL) corresponding to aa 127-137 of H2A.V was coupled to KLH via C-terminal cysteine and used to raise polyclonal rabbit H2A.V antibody (Eurogentec, Netherlands). The specificity of H2A.V antibody was validated by loss of H2A.V immunofluorescence signal upon cell type-specific knockdown with H2A.V shRNA (Figs 6I,M; 7E,G; 8E,I and S6).

Antibodies used in Western blot

The following antibodies were used for Western blot: rat DOA1 17F4 (1:5), mouse DOB2 4H4 (1:5), mouse FLAG M2 (1:5000, F1804, Sigma-Aldrich, Germany), rabbit ISWI (1:1000, kind gift from J. Tamkun, University of California, Santa Cruz, USA) and mouse Lamin T40 (1:3000, kind gift H. Saumweber, Humboldt University Berlin, Germany). mouse (NA931V), rat (NA935V) or rabbit (NA934V) IgG secondary antibodies conjugated to HRP (1:20000, GE Healthcare, UK) and Immobilon Western HRP Substrate (Merck Millipore, Germany) were used for chemiluminescent detection with ChemiDoc Touch Imaging System (Bio-Rad Laboratories, Germany) or X-ray developer machine (AGFA curix 60, Belgium).

Antibodies used in immunofluorescence

The following primary antibodies were used in immunofluorescence: mouse Orb 6H4 (AB_528419) and 4H8 (AB_528418) [1:60, Developmental Studies Hybridoma Bank (DSHB), USA], mouse Fasciclin III 7G10 (1:100, AB_528238, DSHB), mouse UNC93-5.2.1 (γH2A.V, 1:1000, DSHB), mouse Spectrin 3A9 (1:10, AB_528473, DSHB), mouse HP1 C1A9 (1:10, AB_528276, DSHB), rabbit Vasa (1:100, sc-514249, Santa Cruz Biotechnology, USA), rabbit activated Caspase 3 (1:100, 9661, Cell Signaling Technology, USA), rabbit GFP (1:500, TP401, Acris Antibodies, Germany) and rabbit α-H2A (1:200, kind gift of J. Müller, MPI of Biochemistry, Martinsried, Germany). F-actin was visualized with Rhodamine-conjugated phalloidin (1:500, R415, Invitrogen). DAPI (0.1 mg/ml, 1:500) was used to stain DNA. The following secondary antibodies from Jackson Immuno Research Laboratories, INC. were used: Donkey mouse Cy3 (1:250, 715-165-150), Donkey mouse Alexa488 (1:300, 715-545-151), Donkey rat Alexa488 (1:300, 712-485-150) and Donkey rabbit Alexa488 (1:300, 711-545-152). Donkey rabbit Alexa555 (1:250, A-21429) was used from ThermoFisher Scientific, Germany.

Immunological techniques and microscopy

For signal quantification, 8-bit grayscale z-stack images were analyzed with ImageJ software. Area of DAPI-stained nuclei and mean signal intensity were measured for the following cell types: GFP signal in 10 follicle cells (Fig. 2I); H2A.V signal in 30 cysts in region 1, 2 and 3 of the germarium and follicle cells, respectively (Fig. 6E-K); H2A.V signal in 50 nurse and follicle cells of stage 3 egg

chambers, respectively (Fig. 7A-F); H2A.V signal in 50 nurse and follicle cells of stage 8 egg chambers, respectively (Fig. 8A-L) and H2A.V signal in 30 follicle and nurse cells of region 2B, stage 1 and 2, respectively (Fig. 9A-G). Integrated density values were calculated by multiplication of mean signal intensity with corresponding area. For background signal, mean signal intensity was measured and averaged in three adjacent DAPI-signal negative areas. Corrected total cell fluorescence was calculated by subtracting the product of area and average background signal from integrated density values. Mean CTCF values with SD were calculated from three biological replicates.

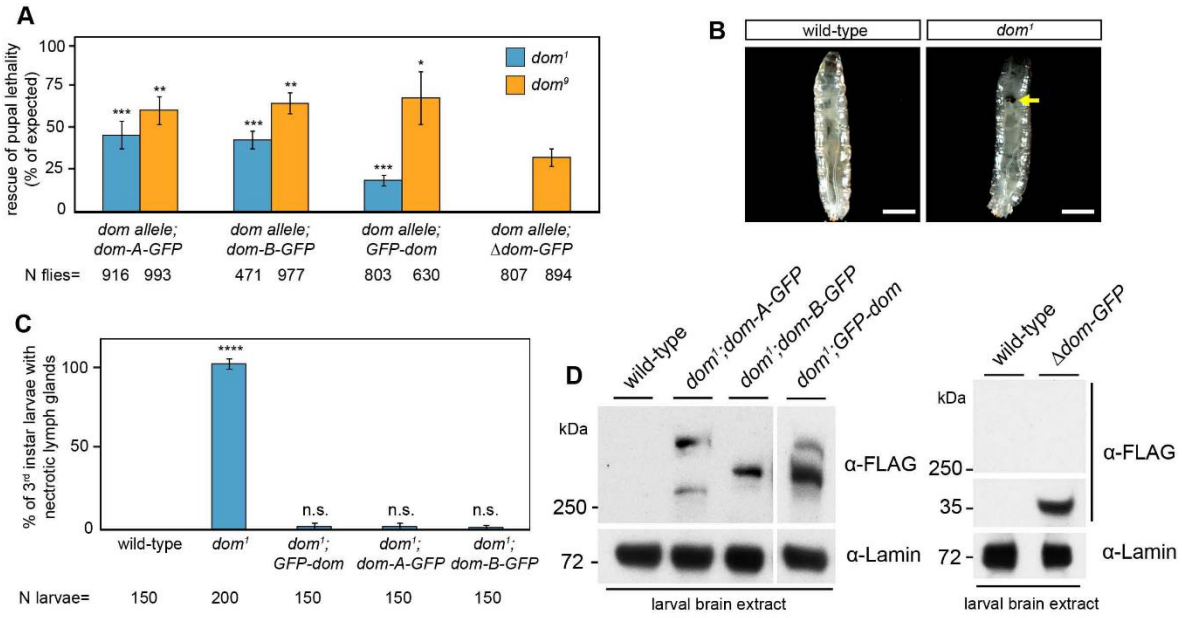

Fig. S1. Characterization of *domino* fosmids

(A) Complementation of *dom* alleles with *dom* fosmids partially rescues lethality phenotype. Rescue of pupal lethality was determined as percentage of observed to expected frequency of homozygous dom^1 or dom^9 offspring. The data show mean values in percentage with s.d. of three biological replicates. *N* represents the total number of scored flies. Two-tailed Student's *t*-test for comparison of dom^1 or dom^9 allele with Δ*dom-GFP*, respectively. **P*<0.05, ***P*<0.01 and ****P*<0.001. (B, C) Complementation of dom^1 allele with *dom* fosmids rescues necrotic lymph glands phenotype. (B) Representative images of 3rd instar larvae are shown for the following homozygous genotypes: wild-type and dom^1. Yellow arrow indicates necrotic lymph glands. Scale bars: 1 µm (C) Quantification of necrotic lymph glands phenotype. The data show mean values in percentage with s.d. of three biological replicates. Two-tailed Student's t-test for comparison with wild-type. *****P*<0.0001; n.s., not significant. (D) Western blot from brains of 3rd instar larvae probed with FLAG antibody is shown for the following homozygous genotypes: wild-type, dom^1;*dom-A-GFP*, dom^1;*dom-B-GFP* and dom^1;*GFP-dom*. Lamin signal provided controls.

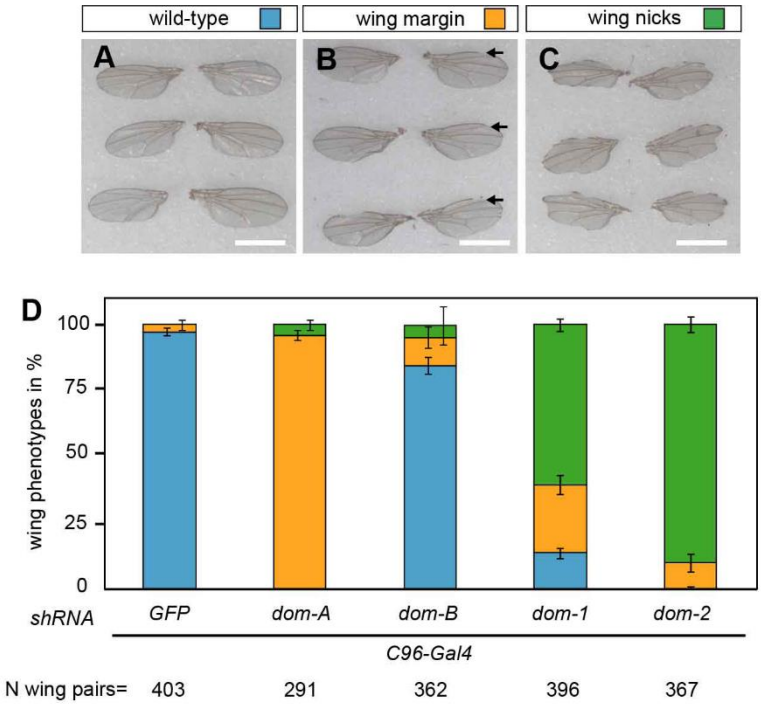

Fig. S2. Depletion of DOM isoforms causes Notch phenotypes in wing development

UAS-shRNA males for *GFP*, *dom-1*, *dom-2*, *dom-A* and *dom-B* were crossed with *C96-Gal4* driver females. (A-C) Wing margin and nick phenotypes were scored in F1 offspring. Black arrow indicates wing margin phenotype. Scale bars: 1 mm. (D) The data show mean percentage with s.d. from three biological replicates. Blue, yellow and green colors indicate wild-type, wing margin and wing nick phenotype, respectively.

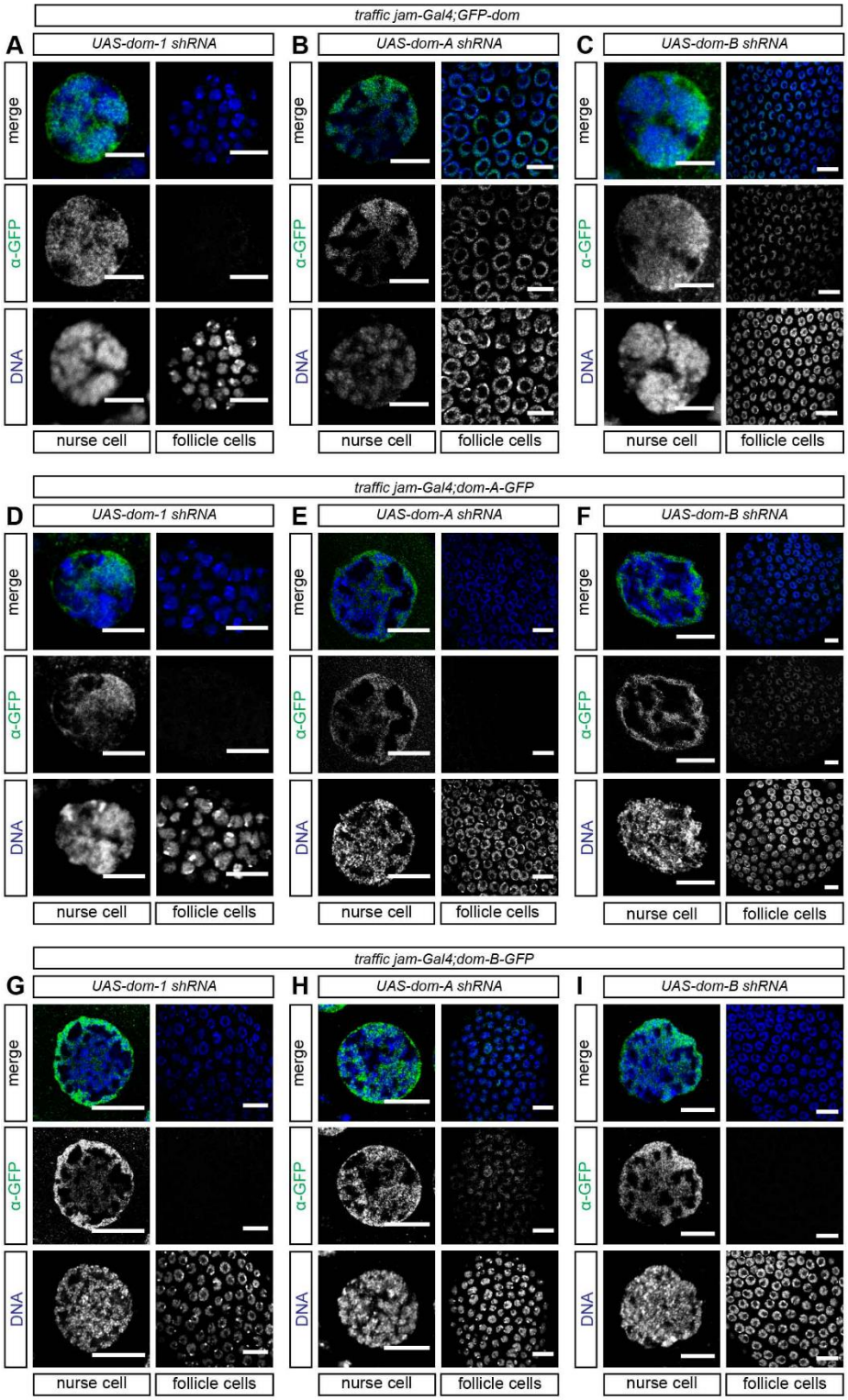

Fig. S3. Validation of cell-type specific knockdown with *dom-1*, *dom-A* and *dom-B shRNAs* and *dom* fosmids

(A-I) Immunofluorescence images of nurse and follicle cells in different stages of oogenesis with staining of GFP (green) and DNA (blue) are shown for the following genotypes: (A-C) *traffic jam-Gal4*;*GFP-dom* with (A) dom-1, (B) dom-A and (C) dom-B shRNA, (D-F) *traffic jam-Gal4*;*dom-A-GFP* with (D) dom-1, (E) dom-A and (F) dom-B *shRNA* and (G-I) *traffic jam-Gal4*;*dom-B-GFP* with (G) dom-1, (H) dom-A and (I) dom-B *shRNA*. Scale bars: 10 µm. Please also refer to Fig. 2 for additional information.

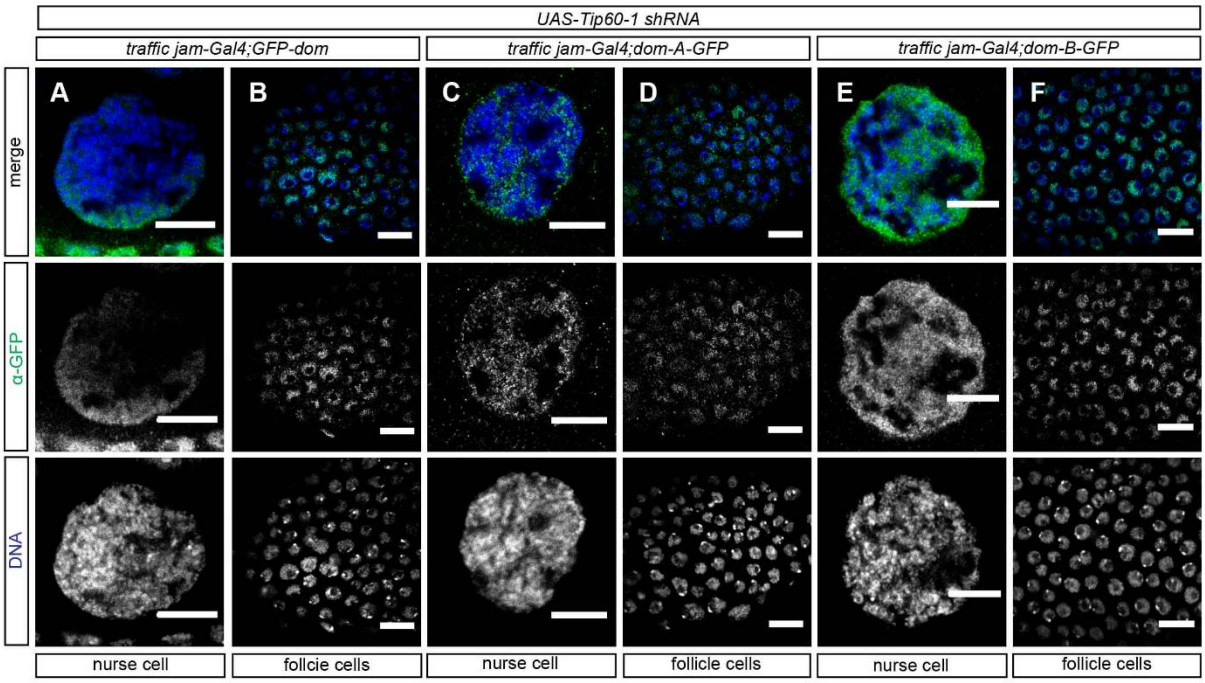

Fig. S4. TIP60 depletion does not affect DOM-A or DOM-B localization in follicle cells

(A-F) Immunofluorescence images of nurse and follicle cells in different stages of oogenesis with staining of GFP (green) and DNA (blue) are shown for the following genotypes: (A-F) UAS-Tip60-1 shRNA with (A,B) *traffic jam-Gal4*;*GFP-dom*, (C,D) *traffic jam-Gal4*;*dom-A-GFP* and (E,F) *traffic jam-Gal4*;*dom-B-GFP*. Scale bars: 10 µm. Please also refer to Fig. 2 for additional information.

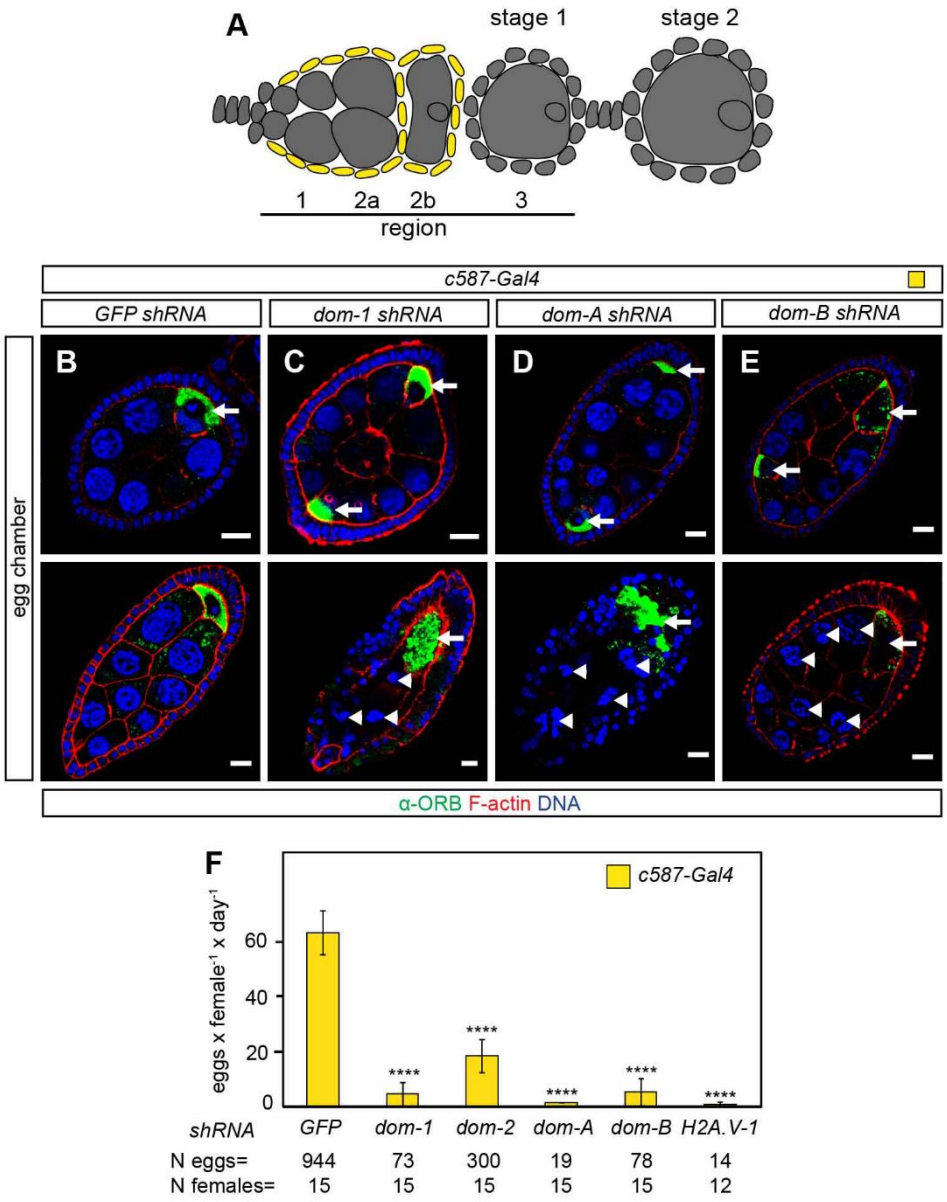

Fig. S5. Validation of packaging defects upon DOM-A or DOM-B depletion with somatic driver *c587-Gal4*

(A) Diagramm of early stages of *D. melanogaster* oogenesis. The specific expression pattern of *c587-Gal4* in somatic escort and follicle cells in the germarium is highlighted in yellow. (B-E) Immunofluorescence images of egg chambers with staining of ORB (green), F-actin (red) and DNA (blue) are shown for the following genotypes: *c587-Gal4* with (B) GFP, (C) dom-1, (D) dom-A and (E) dom-B shRNA. White arrows and arrowhead indicate oocyte and disintegrating nurse cell nuclei, respectively. Scale bars: 10 µm. Staining with the oocyte marker Orb revealed the nature of packaging defects as compound egg chambers with oocytes at opposite positions of an egg chamber and confirmed apoptotic phenotype. (G) Quantification of egg laying capacity. The data show mean values of laid eggs per female and day with s.d. of three biological replicates. *N* eggs represents the total number of scored eggs and *N* females the total number of analyzed females. Two-tailed Student's *t*-test for comparison with GFP shRNA. ****P<0.0001.

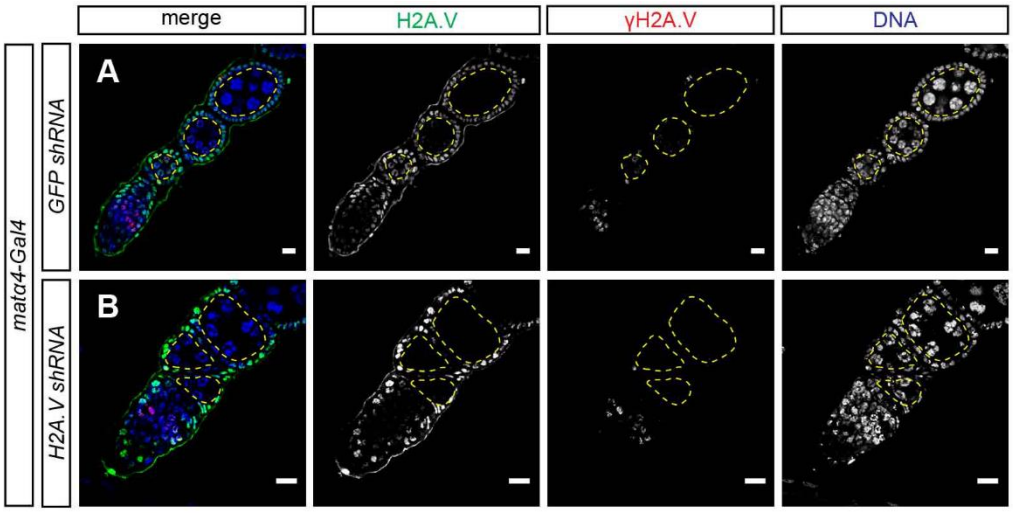

Fig. S6. Characterization of *matα4-Gal4 driver*

(A-B) Immunofluorescence images of ovarioles with staining of H2A.V (green), γH2A.V (red) and DNA (blue) are shown for the following genotypes: *matα4-Gal4* with (A) GFP and (B) H2A.V shRNA. Yellow dashed line indicates germline cells from stage 1 onwards. Scale bars: 10 μm.

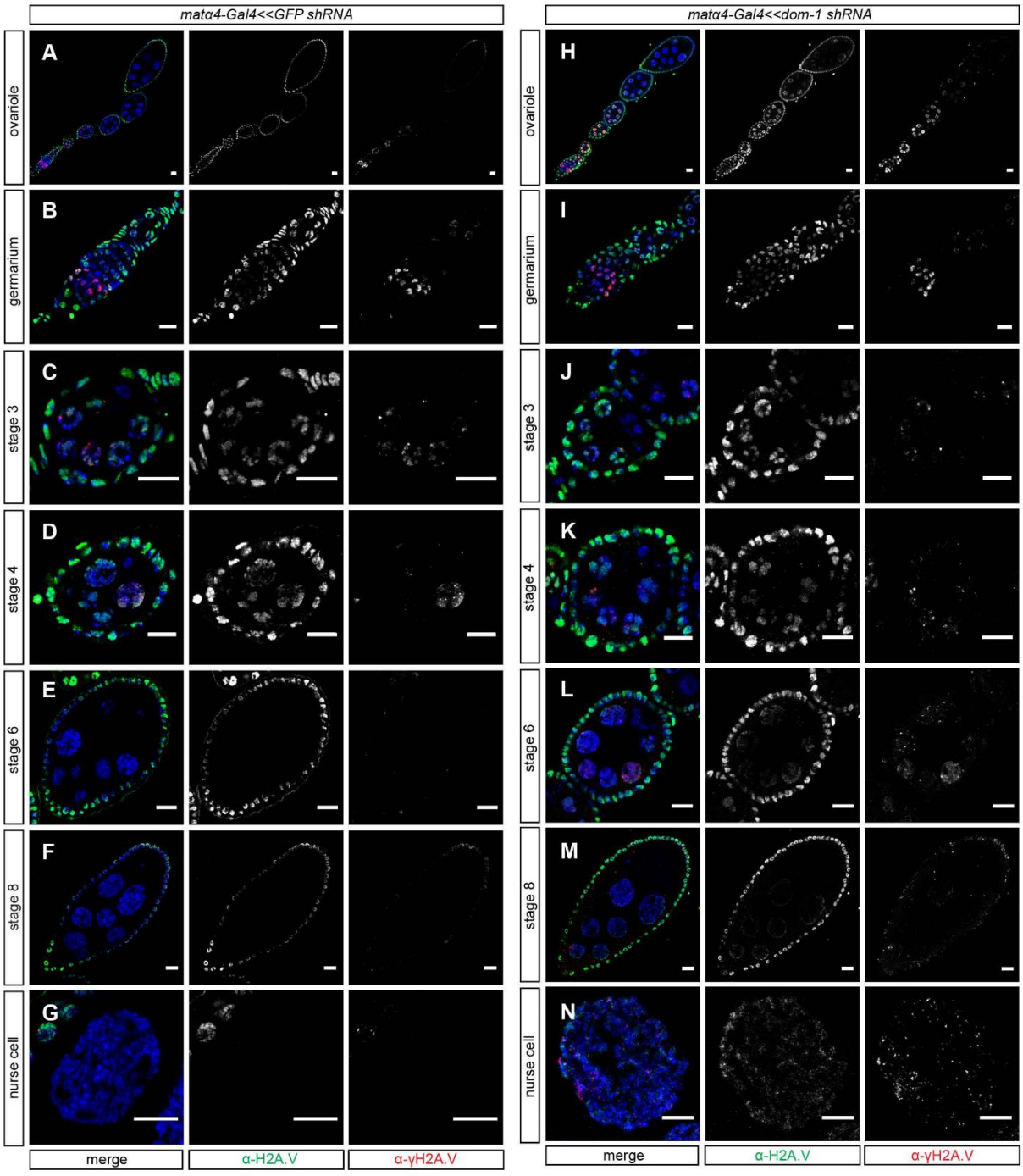

Fig. S7. Loss of DOM in germline cells leads to persistence of H2A.V/γH2A.V from stage 5 onwards

(A-N) Immunofluorescence images of ovariole, germarium, different stages of egg chambers and nurse cell nuclei with staining of H2A.V (green), γH2A.V (red) and DNA (blue) are shown for the following genotypes: *matα4-Gal4* with (A-G) GFP shRNA and (H-N) *d*om-1 shRNA. Scale bars: 10 µm. Please also refer to Fig. 7 and 8 for additional information.

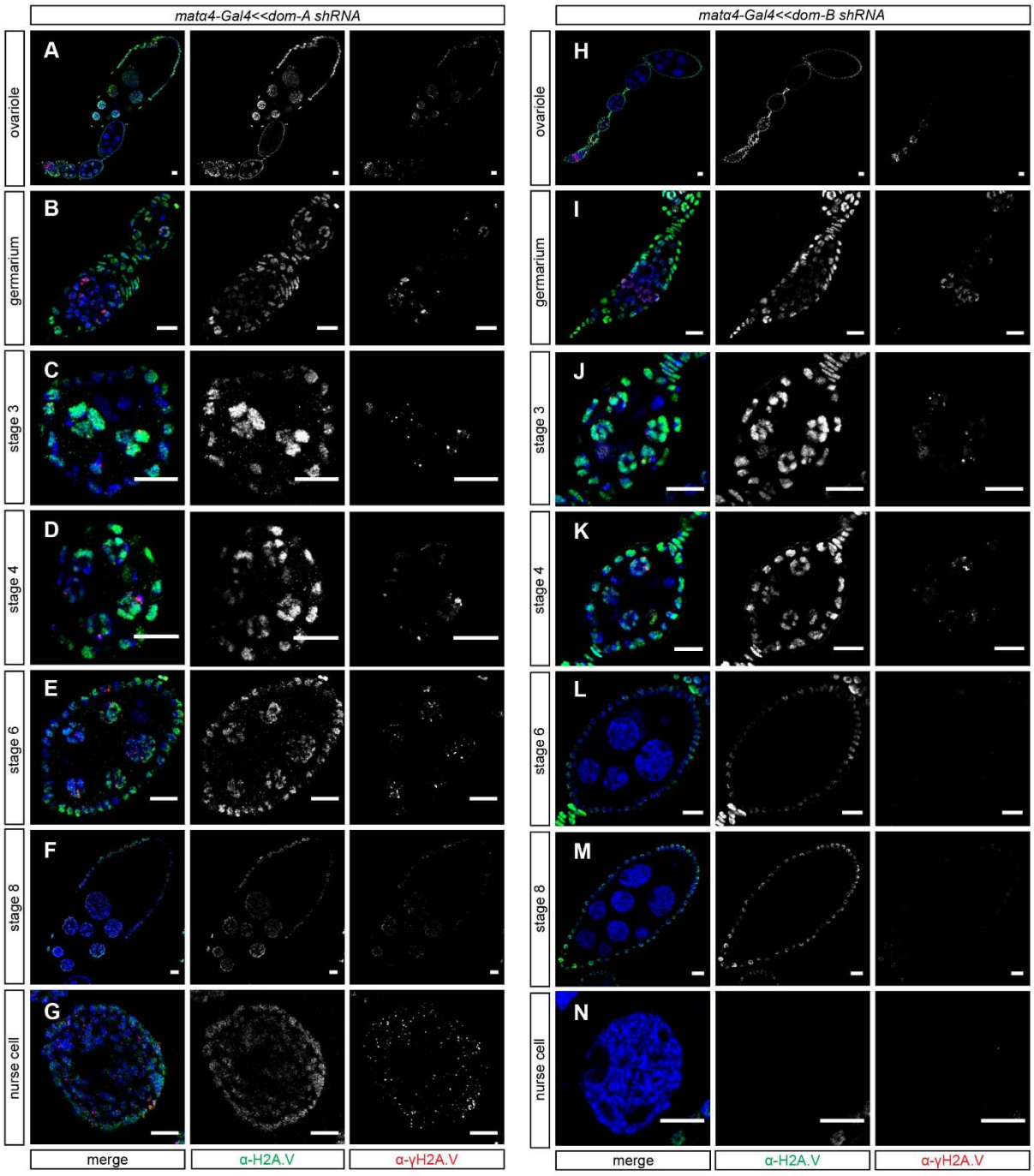

Fig. S8. Loss of DOM-A in germline cells leads to persistence of H2A.V/γH2A.V from stage 5 onwards

(A-N) Immunofluorescence images of ovariole, germarium, different stages of egg chamber and nurse cell nuclei with staining of H2A.V (green), γH2A.V (red) and DNA (blue) are shown for the following genotypes: *matα4-Gal4* with (A-G) dom-A shRNA and (H-N) dom-B shRNA. Scale bars: 10 µm. Please also refer to Fig. 7 and 8 for additional information.

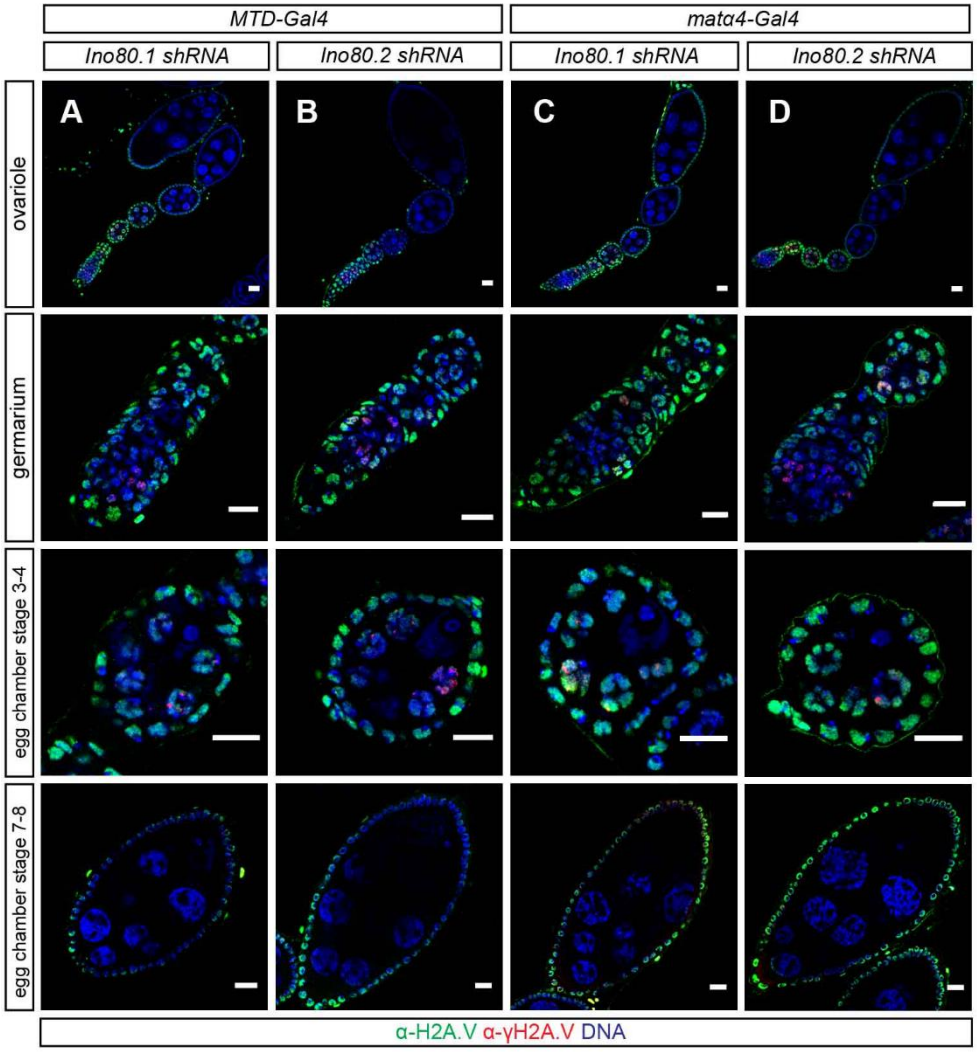

Fig. S9. Germline-specific knockdown of INO80 does not affect H2A.V/γH2A.V association to chromatin

(A-D) Immunofluorescence images of ovariole, germarium and different stages of egg chamber with staining of H2A.V (green), γH2A.V (red) and DNA (blue) are shown for the following genotypes: (A,B) *MTD-Gal4* with (A) Ino80.1 and (B) Ino80.2 shRNA and (C,D) *matα 4-Gal4* with (C) Ino80.1 and (D) *I*no80.2 shRNA. Scale bars: 10 µm.

Table S1. Oligonucleotide sequences used in this study. Please also refer to paragraph '*D. melanogaster* strains and genetics' in Supplementary information for additional information.

Oligonucleotide	Sequence
Dom-rec-N-F	actgtgaactcacacccttctatttttttttgcagatgtctcaaacatggaagtgcataccaatcaggac
Dom-rec-N-R	ggggccgggctgagcccttcatgccccctcctgctgaattaccttcattcttgtcgtcgtcatccttgta
DomA-rec-C-F	aggtacgcaagctggtgcagaaaaagatcctgatacgcagcgagaaagaagaagtgcataccaatcaggac
DomA-rec-C-R	ctcgtgatgctccgccgctgacgtggtctgacggctttagtcgagcgttacttgtcgtcgtcatccttgta
DomB-rec-C-F	cagtcagtggtgtttcgggaggaaatgcctcctcgagcggaacagccagggaagtgcataccaatcaggac
DomB-rec-C-R	aacacacacagctgataatactgactgaggtatgatagtgaacatcatcacttgtcgtcgtcatccttgta

Table S2. Oligonucleotide combinations used in this study. Please also refer to paragraph '*D. melanogaster* strains and genetics' in Supplementary information for additional information.

Transgenic fosmid	Forward Oligonucleotide	Reverse Oligonucleotide
GFP-dom	Dom-rec-N-F	Dom-rec-N-R
dom-A-GFP	DomA-rec-C-F	DomA-rec-C-R
dom-B-GFP	DomB-rec-C-F	DomB-rec-C-R
Δdom-GFP	Dom-rec-N-F	DomA-rec-C-R